https://doi.org/10.5194/egusphere-2026-2918
Preprint. Discussion started: 11 June 2026

Characterizing inertial and diabatic energy transfers in tropical cyclones

Tom Dörffel[1], Natalia Mikula[2], Lisa Schielicke[3], Theresa Kiszler[4], Davide Faranda[5,6,7], Bérengère Dubrulle[8], and Nikki Vercauteren[9]

[1]Leibniz Institute of Atmospheric Physics at the University of Rostock, 18225 Kühlungsborn, Germany
[2]Zuse Institute Berlin, 14195 Berlin, Germany
[3]The University of Western Ontario, London, Ontario, N6A 3K7, Canada
[4]CSC - IT Center for Science, 02150 Espoo, Finland
[5]Laboratoire des Sciences du Climat et de l'Environnement, LSCE/IPSL, CEA-CNRS-UVSQ, Université Paris-Saclay, Gif-sur-Yvette, France
[6]London Mathematical Laboratory, 8 Margravine Gardens, London, W6 8RH, UK
[7]LMD/IPSL, Ecole Normale Superieure, PSL Research University, 75005, Paris, France
[8]SPEC, CEA, CNRS, Université Paris-Saclay, F-91191 CEA Saclay, Gif-sur-Yvette, France
[9]Universität zu Köln, 50969 Cologne, Germany

Correspondence: Tom Dörffel (doerffel@iap-kborn.de)

Abstract. We investigate the multiscale organization of tropical cyclones (TCs) in terms of the redistribution of kinetic energy. In particular, we analyze the across-scale transfer relative to the core scale. Our aim is to find indicators for diagnosing potential events of sudden intensity changes and thereby allowing for a risk-assessment even in cases where dynamical models would not capture the dynamics of the TCs. Two different approaches as diagnostic tools are proposed: a two-dimensional version of the Duchon-Robert index and the leading-order contribution of the diabatic kinetic energy generation. We present results on the analysis of two datasets, one synthetic TC and one extracted from ERA5 reanalyses, and find characteristic patterns of these indicators that are related to the structure and the evolution of the storms. This study serves as a proof-of-concept for future applications of both of the presented indices.

1 Introduction

Tropical cyclones (TCs) rank among the most costly natural disasters worldwide (Munich Re, 2024). Associated high wind speeds and storm surges potentially cause devastating destruction. In the United States of America, TCs stand out economically as the most important natural disaster (Smith and Katz, 2013; Grinsted et al., 2019). Future projections suggest a potential increase in the intensity of TCs in the North Atlantic sector, although with only medium confidence (Kossin et al., 2017; IPCC, 2021). Even the most sophisticated global or regional climate models are not capable of accurately representing the dynamics of severe TCs (Roberts et al., 2020).

Mechanisms that could explain RI and RW can be studied through energetic pathways. The route from weak to strong TCs follows paths of energy transitions across various scales that feed into the vortex scale, ultimately increasing the kinetic energy *i.e.*, the intensity of the TC (Bhalachandran et al., 2020). Energy transitions across scales are connected to symmetric and

https://doi.org/10.5194/egusphere-2026-2918
Preprint. Discussion started: 11 June 2026

asymmetric flow structures. Observations show that events of RI or RW are related to pronounced asymmetries in the flow field and convection patterns (Marks et al., 1992, 2008). There is evidence that symmetric and asymmetric structures are key in explaining energy pathways that lead to intensity changes (Dörffel et al., 2021; Schecter, 2022).

Different approaches have been used to quantify energy transfers. One accounts for the thermodynamics of the system where the storm is converting latent heat into kinetic energy as part of a thermodynamic cycle. Pauluis and Zhang (2017) analyzed the change of equivalent potential energy along Lagrangian fluid trajectories. They restrict to symmetric structures by azimuthally averaging the data effectively considering an axisymmetric storm. Montgomery and Smith (2017a), however, mention that the applicability of symmetric TC models is limited especially in the context of explaining intensity changes. Another approach focuses on kinetic energy transfers across scales, arguing that an upscale transfer of energy activates larger-scale motions, which can enhance the nonlinear interactions between waves and ultimately lead to increases in the mean vortex intensity Sroka and Guimond (2021).

A more general dynamical approach is based on the Lorenz energy cycle (Lorenz, 1955) and analyzes multiple length scales of asymmetric generation of available potential energy (APE) and the conversion to kinetic energy (KE), or conversions of energy across scales. Bhalachandran et al. (2020) define scales by azimuthal Fourier-modes in a cylindrical coordinate system. This spectral approach can disentangle the impact of asymmetries at multiple scales in the spectral domain. Bhalachandran et al. (2020) showed that thermodynamics and asymmetric fluid-dynamical features at different scales could impact TC intensity changes, sometimes with competing effects. They revealed a complex network of directed energy flows between symmetric, low and higher wave-number asymmetric compartments that are responsible for intensification or attenuation.

Asymmetries of the flow fields originate from asymmetries in the environmental conditions, *i.e.*, large-scale wind shear and ocean surface temperature (Wadler et al., 2021). The former leads to pronounced vertical tilt of the vortex center. The tilt can be of the same order of magnitude as the size of the storm itself (Dunkerton et al., 2009; Marks et al., 2008), and this has impacts on the storm dynamics. On the one hand, asymmetries in the vortex-scale flow field (*i.e.* the tilt) have an influence on asymmetries in the boundary layer that lead to asymmetric convection patterns (Alvey et al., 2015; Callaghan, 2017; Frank and Ritchie, 1999; Rios-Berrios, 2020, among others). Asymmetric convection, on the other hand, affects the response of the vortex in terms of tilt and intensity evolution (Li and Dai, 2019; Riemer et al., 2010). Päschke et al. (2012) and a subsequent numerical study (Dörffel et al., 2021) highlight that the geometry of the flow structure interacting with diabatic inhomogeneities will lead to an intensification of the TC. In that theory, the tilt controls how APE is generated and converted to KE during phases of intensification or weakening based on the fluid structural properties.

Many authors who attribute asymmetries in the convection and flow field rely on a cylindrical coordinate system that is centered at a best-guess position of the storm center even in the presence of strong tilts (Nolan and Montgomery, 2002; Nolan and Grasso, 2003; Schecter, 2015; Bhalachandran et al., 2020). The multiscale analyses of the energetic impacts of asymmetries by Bhalachandran et al. (2020) were done in such a coordinate system. It was found that the dominant mechanisms for rapid intensity changes are not only the baroclinic conversion from APE to KE at individual scales of asymmetry, but also the transfers of KE between the asymmetries at various length scales. During RI, they found the conversion of APE to KE to

https://doi.org/10.5194/egusphere-2026-2918
Preprint. Discussion started: 11 June 2026

increase at all scales, concomitant with an upscale KE transfer from high to low wavenumbers. During RW, the APE to KE conversion was decreased, and a dominant downscale KE transfer was found to coexist with a strong upscale transfer.

TCs exhibit a complex turbulence energy spectrum where both downscale (direct) and upscale (inverse) energy cascades can coexist. The direct cascade, a classical Kolmogorov-type transfer of energy from large to progressively smaller eddies, is expected in the intense turbulent flows of the eyewall and boundary layer, leading to dissipation at small scales. Conversely, theory and simulations indicate that part of the convective energy undergoes an inverse cascade, transferring from smaller to larger scales. In a rotating convective system like a TC, small-scale vortices or turbulent eddies can merge or collectively organize, reinforcing the primary cyclone-scale circulation (an upscale growth mechanism analogous to the inverse cascade predicted for 2D turbulence). Observational and modeling studies support this dual behavior: For instance, Hendricks et al. (2004) and Montgomery et al. (2006) showed that "vortical hot towers" (strong convective vortices) in a developing cyclone can aggregate to amplify the nascent cyclone vortex, exemplifying an upscale energy transfer (inverse cascade) during TC genesis. Direct cascades are also evident in high-resolution measurements of hurricane boundary layers, which reveal energy-containing eddies on the order of 1–2 km that break down into smaller turbulent motions. The interplay of these cascades is thought to influence cyclone dynamics: An inverse cascade may contribute to vortex growth and intensification (by energizing larger-scale flow), while the direct cascade governs how energy is ultimately dissipated as heat (affecting the cyclone's energy budget balance). Whether these cascade processes significantly affect our current case depends on the scales and resolution under consideration. In practice, many TC analyses and forecasts (especially those with km-scale or coarser grids) do not explicitly resolve the full inverse cascade; instead, energy upscale effects are partially represented via parameterizations (*e.g.*, stochastic backscatter schemes; Shutts, 2005). In our case, this implies that any inverse cascade effects are likely secondary and implicitly captured, not explicitly dominating the energy budget.

The coexistence of downscale and upscale kinetic energy cascades in TCs was also diagnosed from observational datasets (Byrne and Zhang, 2013; Tang et al., 2015). The parent vortex, once mature enough, imposes a two-dimensional constraint which reduces dissipation and leads to an upscale energy transfer and positive feedback on the vortex strength. These observations, while limited to flight tracks and storm tracks in relation to the location of a measurement tower, show a spatial organization of the inertial energy transfers around the TC structure, with an upscale cascade in the inner-core region of the TC, and above a certain height in the hurricane boundary layer. Very-high-resolution radar measurements of the three-dimensional wind field extended the spatial scope of observational studies and revealed large regions of organized upscale inertial energy transfer (or backscatter) in the boundary layer of Hurricane Rita (2005), associated with coherent turbulent eddies (Sroka and Guimond, 2021). As noted by these authors, few studies investigated the role of the spatial organization of backscatter on the localized dynamics and on the vortex intensity. Using a coarse-graining approach, their analysis focused on periods of peak intensity of the hurricane.

The purpose of our study is to present a proof-of-concept methodology to evaluate the organization of across-scale energy pathways around a tropical cyclone core, thereby acknowledging the importance of the tilted centerline. The study will focus on the combined importance of diabatic and inertial energy transfers. Since we argued that it is merely the vortex tilt that couples to asymmetries of the convection field, we propose to perform the analysis of energy transfers between scales within a

https://doi.org/10.5194/egusphere-2026-2918
Preprint. Discussion started: 11 June 2026

Table 1. Summary and description of the energy transfer indicators. APE: available potential energy, KE: kinetic energy

	physical interpretation	positive (direct)	negative (inverse)
DRI	Scale-wise transfer of kinetic energy from large to small scale (across a given reference scale)	large scale feeds into the small scale, convergence	small scale feeds into the large scale, divergence
Diabatic transfer	Generation rate of APE/KE, partitioned into symmetric and asymmetric contributions	increase of kinetic energy	decrease of kinetic energy

framework where the tilted centerline prescribes the center of rotation per height level and with that the center of a tilted polar coordinate system. Moreover, we aim to study the spatial organization of inertial and diabatic energy transfers around the tilted centerline, without relying on restrictive assumptions inherent to spectral analyses. In particular, the inertial transfers will be mapped using a coarse-graining approach that will enable the evaluation of inertial transfers locally in space and time (Aluie et al., 2018; Faranda et al., 2018).

The paper is organized as follows: In Sec. 2, the definition of a tilted centerline of the TC is introduced, along with a procedure to extract it from gridded datasets. The section further introduces a coarse-graining approach to map inertial energy transfers as well as an approach to evaluate multiscale APE to KE conversions. The idealized TC simulations and the ERA5 case study used to evaluate the energy pathways are introduced in Sec. 3. Sec. 4 presents these energy pathways over the lifetime of the example TCs, and conclusions are given in Sec. 5.

2 Evaluating diabatic and inter-scale energy transfers around a tilted centerline of TCs

The asymptotic model of Päschke et al. (2012) gives rise to the energy budget of the bulk vortex in the free troposphere by attributing diabatic heat release to wavenumbers 0 and 1 that feed into the main (wavenumber-0) circulation (Dörffel et al., 2021). In contrast to canonical approaches (Bhalachandran et al., 2020; Nolan and Montgomery, 2002; Nolan and Grasso, 2003; Reasor et al., 2000, 2004), we propose a modified analysis in that we make use of the notion of a centerline and construct a tilted coordinate system accordingly.

Hence, to analyze the energy pathways in that tilted coordinate system, the definition and extraction of the centerline is key. In section 2.1 we present a method that is applicable and proven to be robust even for non-idealized and coarsely resolved data.

Before going into the detailed descriptions of the methods in the following subsection, and for a better overview, we give a summary of the energy transfer indicators in table 1.

2.1 Defining a tilted centerline of the cyclone

The centerline extraction builds on the extraction of vortex regions. Thereby we define a vortex region with help of the Q-criterion (Hunt et al., 1988; Zhang et al., 2019), also known as Okubo-Weiss number (e.g Tory et al., 2013, for TCs). The

https://doi.org/10.5194/egusphere-2026-2918
Preprint. Discussion started: 11 June 2026

Q-criterion is based on the second invariant Q

$$Q = \frac{1}{2}\left(\|B\|^2 - \|A\|^2\right), \tag{1}$$

of the velocity gradient tensor ∇u where $A = \frac{1}{2}(\frac{\partial u_i}{\partial x_j} + \frac{\partial u_j}{\partial x_i})$ is its symmetric and $B = \frac{1}{2}(\frac{\partial u_i}{\partial x_j} - \frac{\partial u_j}{\partial x_i})$ its antisymmetric component. A vortex is defined as a simply connected region of positive second invariant $Q > 0$. This definition implies that the antisymmetric part dominates in the identified vortex region or in other words that the rotational parts dominate over the deformational parts of the kinematic flow field. This scalar invariant is related to the kinematic vorticity number W_k that was used to identify atmospheric vortices at different scales (Schielicke et al., 2016, 2019).

After the identification of the vortex regions at different tropospheric levels, the centerline is detected by the centroid method proposed in Nguyen et al. (2014); Mikula et al. (2022), using Q as an indicator quantity:

$$\bar{x}(\Omega) = \frac{\sum\limits_{i \in I_\Omega} x_i Q_i}{\sum\limits_{i \in I_\Omega} Q_i} \quad \text{and} \quad \bar{y}(\Omega) = \frac{\sum\limits_{i \in I_\Omega} y_i Q_i}{\sum\limits_{i \in I_\Omega} Q_i}, \tag{2}$$

where i are the indices of horizontal discretization x_i, y_i.

In order to select the vortex regions that correspond to the TC centerline, the normalized pressure perturbation p^* is additionally used for the localization as described by von Lindheim et al. (2021). Vortex regions are then specified by a compound criterion through

$$\Omega = \{x \in \mathbb{R}^3 \,|\, p^*(x) < p_{thr} \text{ and } Q(x) > 0\}, \tag{3}$$

where

$$p^*(x,y,z) = \frac{p(x,y,z) - p_{min}(z)}{p_{max}(z) - p_{min}(z)}. \tag{4}$$

We have $p_{min}(z) = \min_{x,y}(p(x,y,z))$, $p_{max}(z) = \max_{x,y}(p(x,y,z))$ and a pressure threshold value p_{thr}. To ensure that the horizontal slices of Ω form a domain of closed isobars the approach proposed in Mikula et al. (2022); von Lindheim et al. (2021) was used. In addition, the vertical curvature was approximated at every horizontal slice to then discard centerlines that exhibited nonphysical oscillatory behavior. The value of p_{thr} is chosen within the interval $p_{thr} \in [0.851, 0.903]$, where different values are used depending on the height level. These threshold values serve to remove some high p^* values that are outside the domain of closed isobars. Multiple centerlines are identified per time step by applying eq. (2), some of them forming a localized cluster and some that are clear outliers. After selecting the centerlines that form a cluster, the line closest to the cluster center (in terms of Euclidean distance) is chosen as the representative centerline. This approach is motivated more thoroughly on the basis of visual data analysis in Mikula et al. (2022).

2.2 Leading-order APE to KE conversions

Motivated by the asymptotic analysis of a TCs (Päschke et al., 2012; Dörffel et al., 2021), we compute the source terms of the kinetic energy budget (A1). These correspond to APE to KE conversions that lead to intensity changes. We present the

https://doi.org/10.5194/egusphere-2026-2918
Preprint. Discussion started: 11 June 2026

most important details of the mathematical derivation in Appendix A and just refer to the final results here. In the spirit of Lorenz (1955), the resulting expression can be traced back to the correlation of perturbations of potential temperature and vertical velocity (cf. eq. (A8) and Dörffel et al. (2021)). Disentangling the vertical velocity w and the potential temperature perturbation Θ' into symmetric (subscripts $_0$) and antisymmetric (subscripts $_1$) contributions, we obtain the source terms of kinetic energy by integrating over the three-dimensional volume V

$$G = \int_V g\rho \left(\frac{\Theta_0' w_0}{\Theta} + \frac{\Theta_1' w_1}{\Theta} \right) dV \equiv G_0 + G_1 \,. \tag{5}$$

where g is the gravitational acceleration and ρ is density. G_0 and G_1 represent the symmetric and asymmetric source terms of kinetic energy. Note the correlation between Fourier modes of different order cancel due to orthogonality. Päschke et al. (2012) argues that at leading order, w and Θ' do not involve Fourier-modes higher than first in the adiabatic case and, under reasonable constraints on the diabatic heating, also in the diabatic case. Hence, eq. (5) only involves correlations of the zeroth and first Fourier-modes. Evaluating these terms individually, we can attribute growth or decay in the kinetic energy to symmetric and asymmetric heating. For more details on the derivation, we refer to Appendix A.

2.3 Evaluating inter-scale transfers through coarse-graining

In addition to the diabatic energy transfers, we aim to evaluate cascading inertial energy transfers. The diagnostic of inertial energy transfers typically relies on filtering approaches that separate resolved fields from subfilter-scale (SFS) fields, a method initially introduced to the field of turbulence by Leonard (1975). This filtering approach is broadly used in fluid mechanics and in the study of turbulent geophysical flows (Germano, 1992; Meneveau, 1994; Tong et al., 1999; Vercauteren et al., 2008; Vannitsem and Ghil, 2017; Aluie et al., 2018). In all those studies, a filter is applied to the Navier-Stokes equation, thereby highlighting the contribution of the subfilter-scale stress tensor to the filtered (or coarse-grained) velocities. From the obtained governing equation for the filtered velocities, one can derive the energy balance equation for the kinetic energy of the filtered flow and study the contributions of the SFS energy transfers arising due to non-linear interactions (Meneveau, 1994). Using this approach, Sroka and Guimond (2021) diagnosed organized regions of upscale and downscale inertial energy transfers in the TC boundary layer, based on their remotely sensed observations of the wind field during Hurricane Rita (2005).

Based on the weak solution formalism, Duchon and Robert (2000a) showed that energy transfers in a fluid at an arbitrary scale ℓ satisfy a local energy balance equation

$$\partial_t E^\ell + \partial_j \left(u_j E^\ell + \frac{1}{2}\left(u_j \hat{p} + \hat{u}_j p\right) + \frac{1}{4}\left(\widehat{u^2 u_j} - \widehat{u^2} u_j\right) - \nu \partial_j E^\ell \right) = -\nu \partial_j u_i \partial_j \hat{u}_i - \mathscr{D}_\ell, \tag{6}$$

where u_i are the components of the velocity field and p the pressure, $\hat{u}$ and $\hat{p}$ their coarse-grained component at scale ℓ, $E^\ell = \sum_i \rho \frac{\hat{u}_i u_i}{2}$ is the kinetic energy density at scale ℓ (such that $\lim_{\ell \to 0} E^\ell = \rho u^2/2$), with ρ being the fluid's mass density. The Duchon-Robert Index (DRI) $\mathscr{D}_\ell$ is expressed in terms of velocity increments $\delta \boldsymbol{u}(\boldsymbol{r}, \boldsymbol{x}) \overset{def}{=} \boldsymbol{u}(\boldsymbol{x}+\boldsymbol{r}) - \boldsymbol{u}(\boldsymbol{x}) \equiv \delta \boldsymbol{u}(\boldsymbol{r})$ (the dependence on ℓ and $\boldsymbol{x}$ is kept implicit) as:

$$\mathscr{D}_\ell(\boldsymbol{u}) = \frac{1}{4\ell} \int_{\mathcal{V}} d\mathcal{V} \, (\boldsymbol{\nabla} \mathcal{G}_\ell)(\boldsymbol{r}) \cdot \delta \boldsymbol{u}(\boldsymbol{r}) \, |\delta \boldsymbol{u}(\boldsymbol{r})|^2. \tag{7}$$

https://doi.org/10.5194/egusphere-2026-2918
Preprint. Discussion started: 11 June 2026

In this definition G is a smooth filtering function, non-negative, spatially localized and such that $\int d\mathcal{V}\, \mathcal{G}(\boldsymbol{r}) = 1$. The function G_ℓ is rescaled for a given volume with ℓ as $\mathcal{G}_\ell(\boldsymbol{r}) = \ell^{-3} G(\boldsymbol{r}/\ell)$. While the choice of $\mathcal{G}_\ell$ may impact the local energy budget evaluation, previous analyses have shown a limited impact (Kuzzay et al., 2017).

In the following application, the calculations are done on horizontal slices for vertical levels, hence on two-dimensional data.[1] This is a viable approach to simplify the calculation since generally the horizontal velocity dominates over the vertical component by at least two orders of magnitude (Klein, 2010; Päschke et al., 2012; Dörffel, 2022). Further note that due to the 2D horizontal filtering approach, we may omit variations of ρ due to the vertical stratification in the integral in eq. (7) as it appears as a prefactor.

The DRI is an inter-scale flux term, describing how the energy locally cascades across the length scales (Dubrulle, 2019). $\mathscr{D}_\ell > 0$ ($\mathscr{D}_\ell < 0$) correspond to a downscale (upscale) transfer of energy relative to the filter scale ℓ (cf. table 1). By construction, the intrinsic weak formulation of $\mathscr{D}_\ell$ makes it less sensitive to noise than the classical coarse-graining approaches discussed above. Indeed, the derivative in scale is not applied directly to the filtered velocity fields, but rather on the smoothing function, followed by a local angular averaging. Possible noise coming from the estimate of the velocity increments is averaged out by the angular averaging (Kuzzay et al., 2015). This method was used to study subfilter-scale energy transfers in atmospheric flows (Faranda et al., 2018) and will be used in our subsequent analyses. The filter scale used for the analyses is $30\,\mathrm{km}$ which corresponds to a sub-vortex scale (Päschke et al., 2012; Dörffel et al., 2021; Dörffel, 2022). Following the aim to study the organization of inertial transfers according to the structure of the hurricane, the results will be visualized based on a coordinate system centered on a tilted centerline.

3 Tropical cyclone data

The diabatic and inertial energy transfers are evaluated for two datasets. The first dataset is obtained from idealized simulations of TCs within a controlled environment. Results of its analysis are presented in section 4.1. The second dataset stems a case study based on hurricane Florence using ERA5 reanalysis data (Hersbach et al., 2020) with results being presented in section 4.2. For each case the structural organization of both energy pathways is compared with each other in section 4. In the following, we give an overview description of the two datasets.

[1] The 2D filter is adapted from Kuzzay et al. (2017) as a circular symmetric filtering function of the scalar increment r given by

$$G_\ell(r) = \begin{cases} \frac{1}{N}\exp\left(-\frac{1}{1-(r/2a)^2}\right), & \text{if } r < 2a\,, \\ 0, & \text{otherwise}\,, \end{cases} \tag{8}$$

where N is a normalization constant. By numerical quadrature, it is evaluated as $N = 0.80793$ for the given study. The derivative of (8) takes its minimum at $r = \pm\frac{2a}{\sqrt[4]{3}}$. In our computations $a = 0.658$ was used, hence setting the minimum at $r = 1$. This choice ensures that for dimensional units, the maximum weight for the computation of $\mathscr{D}_\ell$ is given at the filter scales.

https://doi.org/10.5194/egusphere-2026-2918
Preprint. Discussion started: 11 June 2026

3.1 Idealized tropical cyclones

The diabatic and inertial energy transfers are first investigated for an idealized TC in a sheared environment, based on a simulation using Cloud Model 1, Version 20.2 (CM1, Bryan and Fritsch, 2002). CM1 is a convection-permitting, non-hydrostatic, moist numerical model that is designed for idealized studies of atmospheric phenomena such as thunderstorms, TCs, squall lines, orographic waves, or sea breezes (e.g. Bryan and Fritsch, 2002; Schielicke et al., 2024). In this work, we use the preconfigured 3d hurricane test case (mostly following Bryan, 2012) with a modified vertical wind profile to enable vertical wind shear. The TC develops in an environment initialized by the "Moist Tropical" sounding from Dunion (2011) with a sea surface temperature of 28°C. Weak shear is introduced to the original environment with 2 m/s wind from the east close to the surface and 2 m/s west wind at about 11 km height, and constant above (see Tab. 2). This magnitude of vertical wind shear is within the range observed to favor (significant) intensification (Paterson et al., 2005). The domain size is $3000\,\mathrm{km} \times 3000\,\mathrm{km}$ in the horizontal direction, discretized by 384×384 grid points. In the vertical, we have 59 levels with $z_{\mathrm{top}} = 25\,\mathrm{km}$. The horizontal grid has a constant grid spacing of 4 km in the inner domain up to a radius of 560 km and is then stretched to 16 km outside. The vertical grid is also stretched with 50 m grid spacing at the surface that increases gradually to 500 m at 5.5 km and above. The lateral boundary conditions in all directions are periodic. Coriolis acceleration is considered on an f-plane with $f = 5 \cdot 10^{-4}\,\mathrm{s}^{-1}$. Atmospheric radiation is approximated by a relaxation term following Rotunno and Emanuel (1987). The simulation runs over 8 days with an hourly output. The vortex is initialized by a cyclonic wind field associated with a modified Rankine vortex with maximum tangential winds of 15 m/s at 75 km around the center of the domain. Convection is triggered by randomly distributed warm bubbles and a warm core are added to the cyclonic wind field. Over time, a mature tropical cyclone evolves (>100 h into the simulation) with constant maximum wind speeds of about 70 m/s (category 4–5 on the Saffir–Simpson scale) between about 100 h and 140 h into the simulation. Thereafter, the TC weakens to about 50 m/s maximum winds (categories 2–3) at 150 h and then intensifies again over the next 30 hours, again reaching 70 m/s maximum winds.

Table 2. Vertical wind profile ($\boldsymbol{v} = (U, V)^T$) in idealized CM1 simulation of an idealized TC in a sheared environment (thermodynamical profile is based on the "Moist Tropical" sounding of Dunion (2011))

Height (m)	124	810	1541	3178	4437	5887	7596	9690	10949
U (m/s)	-2.0	-1.5	-1	-0.5	0.0	$+0.5$	$+1.0$	$+1.5$	$+2.0$
V (m/s)	0.0	0.0	0.0	0.0	0.0	0.0	0.0	0.0	0.0

3.2 Hurricane Florence as a case study

Next to the idealized data, we apply the methods to historic tropical cyclone data. To this end, we selected Florence (2018) which exhibits some interesting features throughout its development, in particular such features that are related to environmental wind shear and rapid intensity changes. Below, we give a brief description on the history of the storm and the ERA5 reanalysis data (Hersbach et al., 2020).

https://doi.org/10.5194/egusphere-2026-2918
Preprint. Discussion started: 11 June 2026

On August 28, 2018, the National Hurricane Center began monitoring a tropical wave located over West Africa for possible tropical cyclogenesis over the next five days (Stewart and Berg, 2019). At the end of August 31, while south of Cape Verde, the disturbance was classified as a tropical depression, and at 09:00 UTC on September 1, it officially became a tropical storm, receiving the name Florence. On September 4, at 15:00 UTC, the storm became a Category 1 hurricane on the Simpson and Saffir (1974) scale, while located about 2 000 km west-northwest of Cape Verde. Florence underwent a rapid intensification, becoming a Category 3 hurricane at 12:35 UTC on September 5, and a Category 4 hurricane at 21:00 UTC, with winds up to 215 km/h and a minimum central pressure of 953 mbar. This rapid intensification was associated with a change in trajectory of the storm towards the north, where a persistent vertical wind shear caused the hurricane structure to rapidly degrade beginning on September 6, and at 03:00 UTC on September 7, Florence weakened to a tropical storm. On September 9, Florence again strengthened to a Category 1 hurricane, with sustained winds of 122 km/h. Fueled by sea surface temperatures of 29-29.5 °C and a favorable outflow, Florence then rapidly intensified again, becoming a Category 4 hurricane with sustained winds of 215 km/h and a minimum central pressure of 946 mbar at 16:00 UTC on September 10. At 21:00 UTC, the hurricane reached its peak intensity, sustaining winds of 220 km/h and a minimum central pressure of 939 mbar. Subsequently, the eyewall replacement cycle led Florence to temporarily weaken to a Category 3, before strengthening again to a Category 4 hurricane in mid-September 11. On September 12, Florence began to weaken again due to a moderate wind shear. Throughout September 13, the first rainfall and hurricane-force winds began to make landfall at the cost of North Carolina. At 03:00 UTC on September 14, while the eye was about 95 km from the city of Wilmington, Florence was downgraded to a Category 1 hurricane. Shortly thereafter, at 11:15 UTC, the hurricane made landfall on the North Carolina coast near Wrightsville Beach, with sustained winds of 150 km/h and a minimum central pressure of 958 mbar.

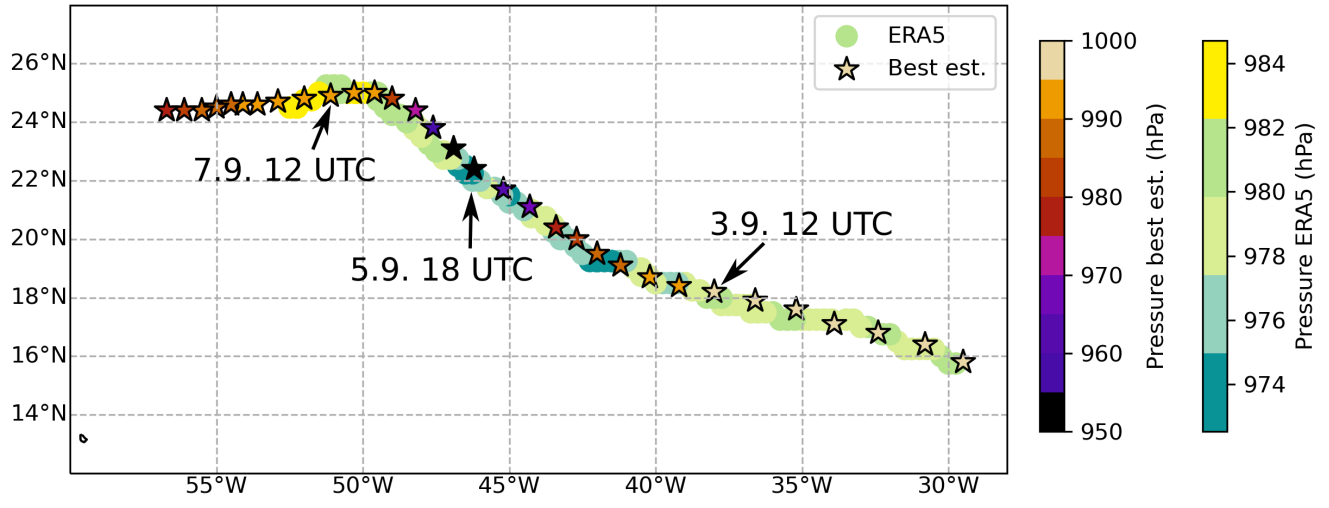

Figure 1. Track of the hurricane Florence computed from the ERA5 reanalysis (dots) and the best estimate (stars). The minimum pressure at sea level is colored as indicated. Times which are important for the analysis are highlighted.

https://doi.org/10.5194/egusphere-2026-2918
Preprint. Discussion started: 11 June 2026

The track, presented in Fig. 1, aligns very well with that of the HURDAT2 database (Landsea and Franklin, 2013). This database provides the best estimates of cyclones tracks/intensity every 6 h, as well as for special intensity reports points such as landfalls, intensity peaks in terms of minimum pressure, extreme winds or changes of status of the cyclones. ERA5 reproduces some of the qualitative intensity features of Florence, albeit not as pronounced and with less variability in minimum surface pressure than estimated from the HURDAT2 database (see fig. 1). This underestimation of the intensity has been found to be common in several reanalysis datasets and is reasoned to be caused by too low model resolutions as well as insufficient sub-grid scale parameterizations Hodges et al. (2017). The decay phase of the cyclone is well captured by the reanalysis.

For the subsequent analysis the data is mapped to height-levels using the toolbox `wrf-python` (Ladwig, 2017).

4 Results

In the following section we present the results of applying both methods, presented in section 2, to both datasets of section 3. Section 4.1 we present results on the idealized storm and in section 4.2 those of the ERA5 reanalysis data of Florence (2018).

4.1 Idealized scenario with weak vertical shear

We begin the analysis by evaluating the inertial energy transfers in section 4.1.1 and continue presenting the results of the diabatic transfer analysis in section 4.1.2.

4.1.1 Inertial energy transfers in the idealized scenario

For the idealized TC (cf. section 3.1), we present in fig. 2 the vertical slices of the horizontal average of the DRI, given in eq. (7), at a scale length of 30 km over time. The 30 km scale is chosen on the basis of the vortex core size.

In general, we find a threefold structure of the energy transfer present throughout all time steps: (i) On top of the storm, *i.e.*, at the tropopause, we observe negative (upscale) energy transfer corresponding to the divergent outflow of the TC's secondary circulation. (ii) The mid-troposphere is characterized by dipolar structures with low-amplitude horizontal mean. (iii) The most prominent feature, however, is the positive (downscale) energy transfer in the boundary layer near the ocean surface. Here, the DRI takes the largest absolute values. We organize the subsequent discussion along this vertical organization from ground to top.

Comparing the horizontal-mean DRI over positive values within the first 1.5 km of the atmosphere (solid red curve in fig. 2) with the maximum wind speed $v_{\max}$ (black curve), we observe a correlation of DRI and intensity within the boundary layer. The correlation is quantified in fig. 3 resulting in a Spearman's rank correlation coefficient (Spearman, 1904) of $\rho = 0.87$.

During the phase of intensification ($dv_{\max}/dt > 0, t \in [25\,\mathrm{h}, 100\,\mathrm{h}]$), the positive inertial energy transfer in the boundary layer builds up. The DRI continues to intensify (100–140 h) until it reaches a maximum right before the storm starts to weaken. In the subsequent weakening phase (140–150 h) both, the intensity of the storm and the inertial energy transfer in the boundary layer diminish, and re-emerge during the following intensification phase (160–180 h). With the lower panel of fig. 2, we further focus on the weakening phase between 140 and 150 h and the subsequent intensification between 150 and 180 h as it gives

https://doi.org/10.5194/egusphere-2026-2918
Preprint. Discussion started: 11 June 2026

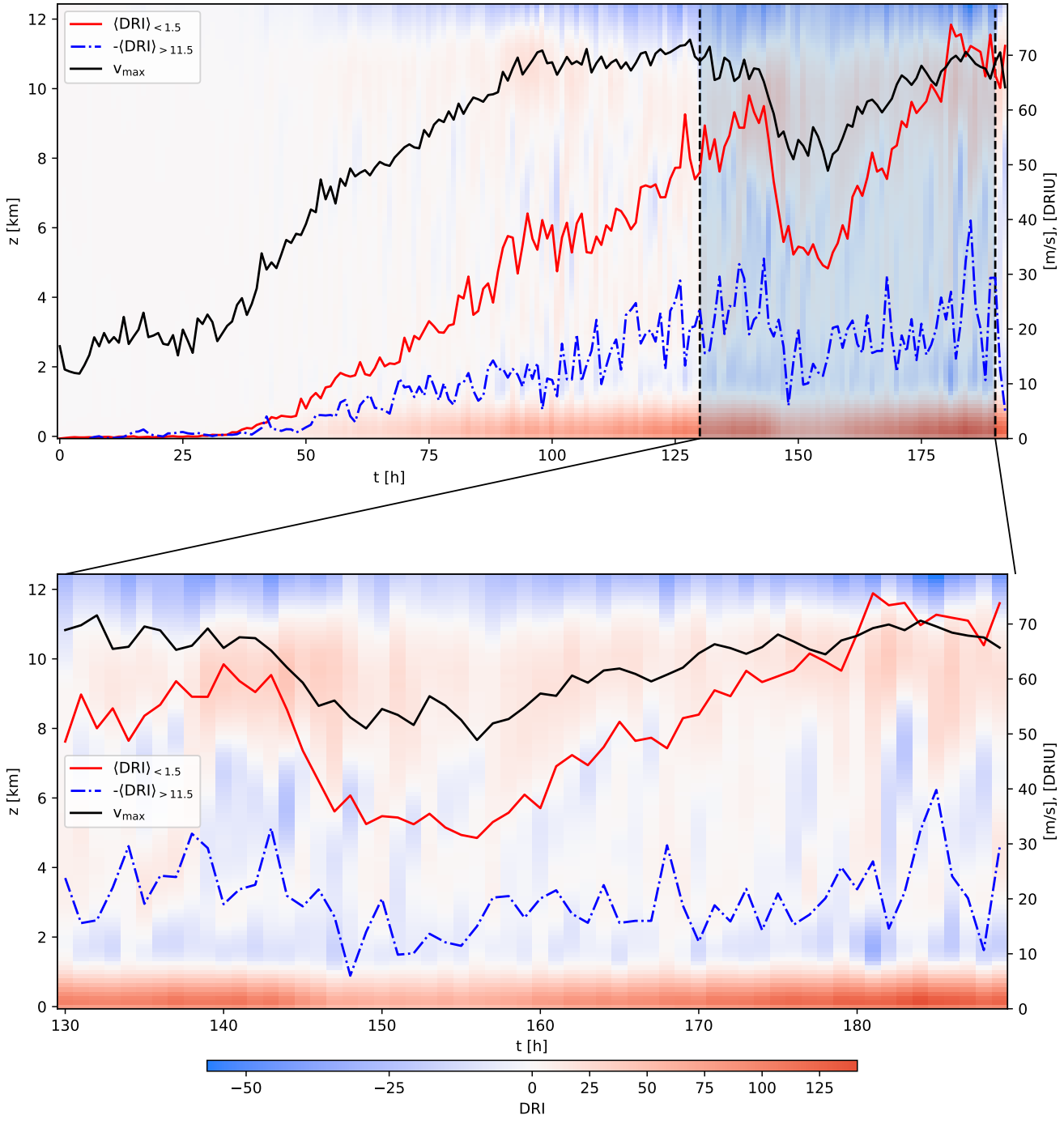

Figure 2. DRI of an idealized TC in a slightly sheared environment: DRI values at a filter scale of 30 km for the entire period (top) and for a sub-interval (130–180 h, bottom). In both figures, the horizontal-mean values are color-coded as t-z plot with the corresponding axes located at bottom and left. The magnitude is given by the colorbar in normalized units. Additional information is given by the time-dependent vertical average of all positive DRI values over the first 1.5 km (solid red line) and all negative DRI values for $z > 11.5$ km (dash-dotted blue line). Both time series use the red axis on the right. Lastly, the maximum wind speed is given by the black line with values again indicated by the black axis on the right.

https://doi.org/10.5194/egusphere-2026-2918
Preprint. Discussion started: 11 June 2026

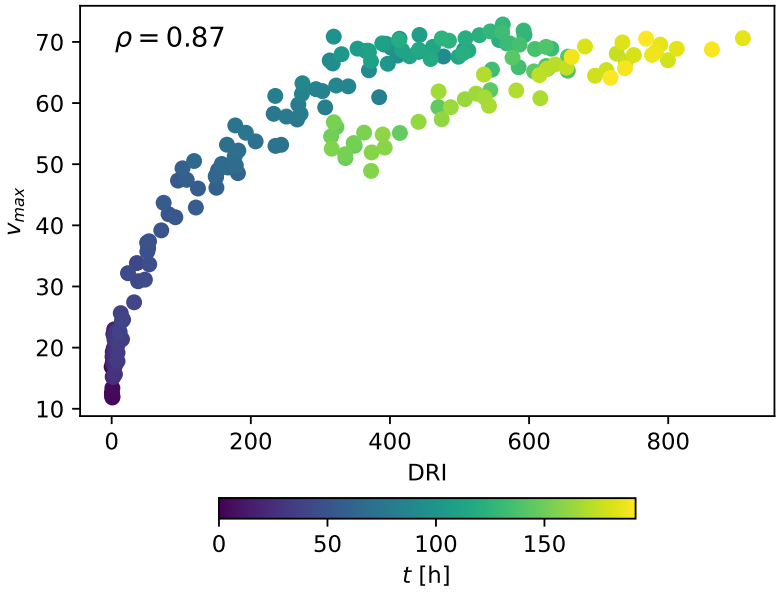

Figure 3. Scatter plot of correlation between positive DRI values measured at the lowest $1.5\,\mathrm{km}$ and v_{max}. The color code indicates the time evolution of the values and the Spearman's correlation coefficient is given by ρ.

interesting insights into the interplay of the DRI structures with the structure of the storm. The weakening of the storm is accompanied by a weakening of the boundary layer's positive energy transfers.

We also notice that the height of the zero-level varies over time. The most significant impact happens at the time the storm is the weakest at the end of the weakening phase (approx. $150\,\mathrm{h}$). In the subsequent re-intensification phase, this height oscillates around the level before the weakening phase. The time series of the average DRI across the first $1.5\,\mathrm{km}$ of the troposphere supports this picture (red curve in fig. 2). As for the very definition of the DRI, namely accounting for across-scale energy fluxes at the scale length of $30\,\mathrm{km}$, we interpret the signal as the frictional low-level convergence of air masses that carry kinetic energy and momentum with them.

Averaging the DRI values with a mask selecting only positive values in the lower $1.5\,\mathrm{km}$ of the atmosphere at first may seem somewhat arbitrary. We argue, however, that the positive values of DRI, *i.e.*, converging air masses near the ground are, in fact, what constitutes the boundary layer. Masking for positive values allows us to capture the temporal evolution of the boundary layer top, *i.e.*, the height where DRI changes its sign. This viewpoint is in congruence with recent asymptotic analyses of tropical cyclones (Dörffel et al., 2026). In fact, by focusing on the $30\,\mathrm{km}$-scale for the DRI we do not account for turbulent transport but rather on the organization of vortex core-scale motions.

Figure 4 reveals the three-dimensional structure of the DRI values taken around the storm at six given time steps. Along the lines of the previous findings, the presented structures are again composed essentially of three parts: (i) On top of the storm near

https://doi.org/10.5194/egusphere-2026-2918
Preprint. Discussion started: 11 June 2026

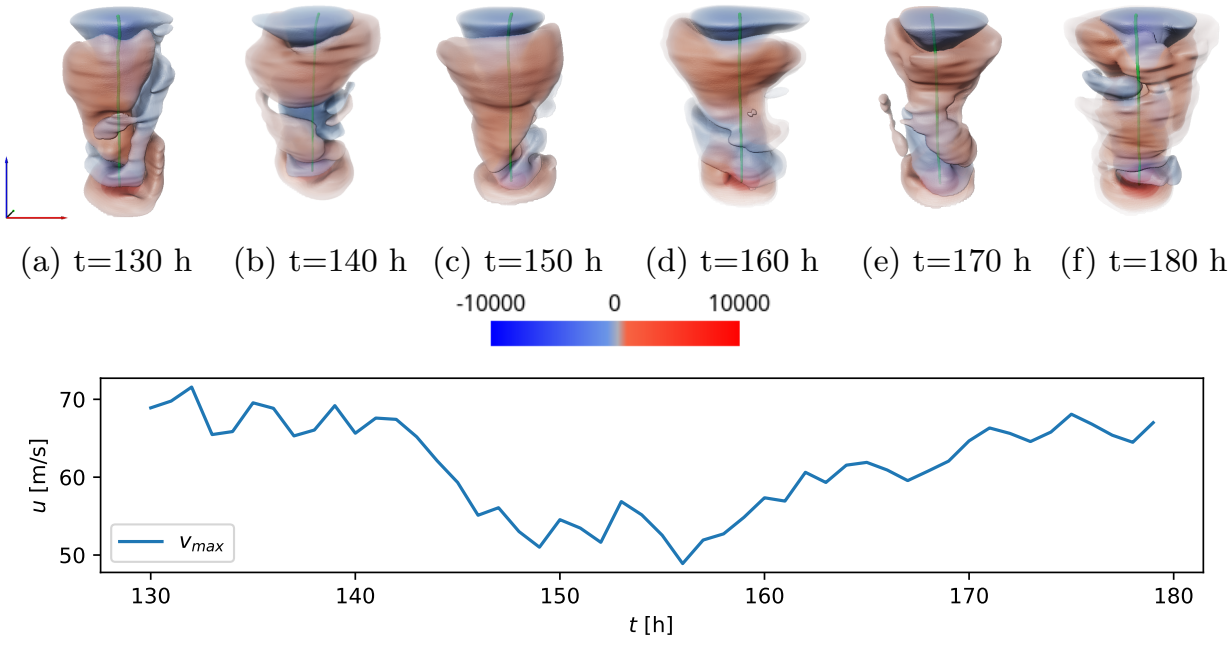

Figure 4. Smoothed 3D structures that represent DR indicator values at 30 km scale computed for idealized simulation with shear wind for time frames 130 to 180 h. The green line represents the centerline of the TC. For reference, the time series of $v_{\max}$ is given in the bottom panel.

the tropopause a region of negative DRI forms. (ii) In the mid-troposphere positive and negative DRI structure of wavenumbers 1 and 2 emerge. (iii) We observe a disk of positive DRI connected to the converging air masses in the frictional boundary layer.

In the mid-troposphere above the boundary layer, the DRI organizes along the centerline and forms dipolar and quadrupolar structures (see top-row of fig. 4). These quadrupolar structures partially explain the low amplitude of the mid-atmosphere signal observed in fig. 2. Next to the relatively low amplitude, canceling of positive and negative contributions are what causes the average signal in to be so weak. We have almost equipartition of positive and negative DRI with a bias slightly to the positive side.

In fig. 5 we analyze the positive mean-DRI contributions in the mid-troposphere between 7 and 11 km. While low values of DRI coincide with phases of continuous intensification, the high values can be associated with the onset of stagnation (100 h) or, in case of the stronger burst at 140 h, with attenuation. The three-dimensional visualizations of fig. 4 during these phases show the emergence of a dominant symmetric structure in the upper mid-troposphere. We observe, that during the intense phase (fig. 4a,b, just before attenuation), positive and negative contributions concentrate towards the center of the storm, while the weakening phase (fig. 4c,d) is accompanied by wider dipole DRI structures, which re-focus during the subsequent intensification (fig. 4e,f). It remains open what might be the physical origin of this signal. Typically, numerical models parameterize

https://doi.org/10.5194/egusphere-2026-2918
Preprint. Discussion started: 11 June 2026

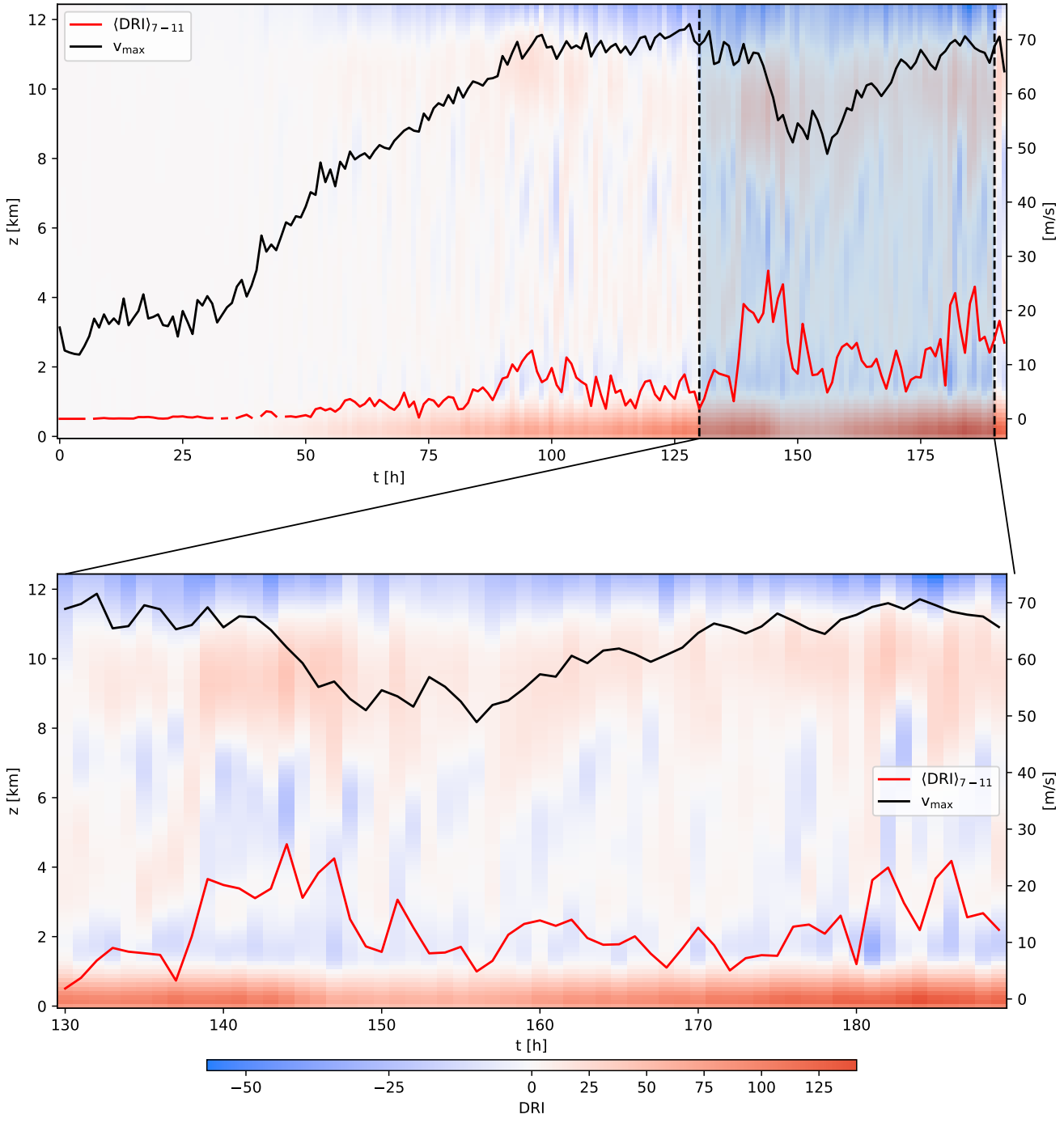

Figure 5. Same as fig. 2, but for the positive DRI values in the mid-troposphere between 7 and 11 km.

https://doi.org/10.5194/egusphere-2026-2918
Preprint. Discussion started: 11 June 2026

entrainment and detrainment as part of the cloud-convection scheme. What we see here might be the residual flow of competing entraining and detraining air masses (Dörffel et al., 2026; Montgomery and Smith, 2017b; Smith and Montgomery, 2024; Gregory, 2002).For the secondary circulation to establish we need convergence (enhanced through entrainment) in the lower parts of the troposphere and divergence in the upper parts (enhanced through detrainment). Entrainment in the upper troposphere might counteract and partially cancel this circulation and thus lead to stagnation or attenuation. However, a profound investigation of this topic would require more high-resolution data.

Finally, we notice stronger negative inertial energy transfer, corresponding to outflow, in the upper troposphere during phases of higher intensity and negative DRI values lower in amplitude during weaker phase of the TC. The dash-dotted blue line in fig. 2 shows average over the negative DRI values above $11.5\,\mathrm{km}$ with a similar behavior as for the positive DRI in the boundary layer, but with lower absolute values. We interpret these structure as the top-level anticyclone that is characteristic for mature TCs.

4.1.2 Diabatic transfers in the idealized scenario

We continue by analyzing the diabatic transfer (eq. (5)) as accounted for by the asymptotic theory of Päschke et al. (2012); Dörffel et al. (2021, 2026). Similar to the previous DRI discussion, we present results in figs. 6 and 7. This quantity corresponds to the kinetic energy increase due to the symmetric and the asymmetric diabatic heating. While the DRI analysis reveals pronounced signals in the boundary layer, here we observe signals of diabatic transfer mostly in the bulk of the troposphere. Nevertheless, the signal show qualitative similarities to the DRI analysis of fig. 2.

In fig. 6, we first observe that the gradual increase between $40\,\mathrm{h}$ and $100\,\mathrm{h}$ is accompanied by an increase in intensity that eventually saturates between 100 and $140\,\mathrm{h}$. After the initial period of intensification, an event of suppressed diabatic energy transfer occurs that is accompanied by a decrease in maximum wind speed, which ultimately recovers at $180\,\mathrm{h}$ into the simulation. Through fig. 7, we find a significant monotonous correlation between intensity and diabatic transfer of $\rho = 0.85$ (with $p < 0.05$), at least below the saturation of intensity. After the peak intensity of about $70\,\mathrm{m/s}$ a further increase in diabatic transfer does not lead to a further increase in intensity.

With the asymptotic theory of Päschke et al. (2012); Dörffel et al. (2021), we are able to dissect the diabatic transfer into a symmetric and an asymmetric part. The Fourier-0 contribution G_0 (not shown here) closely resembles the combined visualization presented in fig. 6, as the Fourier-1 modes contribute only marginally in the present case. To examine the role of the Fourier-1 contribution G_1, we present it in fig. 8. The amplitude of the signal is about one order of magnitude smaller than G_0. In the mid-troposphere we observe, however, at least two imprints of negative bursts in the weakening phase (lower panel of fig. 8, one between $130\,\mathrm{h}$ and $140\,\mathrm{h}$, and a weaker one between $150\,\mathrm{h}$ and $160\,\mathrm{h}$). Both can be associated to episodes of intermittent weakening. More in-depth correlation analysis of the signal, however, did not reveal further insights.

We interpret the role of Fourier-mode-0 diabatic heating, at least in the present case, as the main driver for intensification and as the counteracting mechanism to friction, and we observe a positive correlation between Fourier-mode-0 heating and intensity: With higher wind speeds also the symmetric energy input increases.

https://doi.org/10.5194/egusphere-2026-2918
Preprint. Discussion started: 11 June 2026

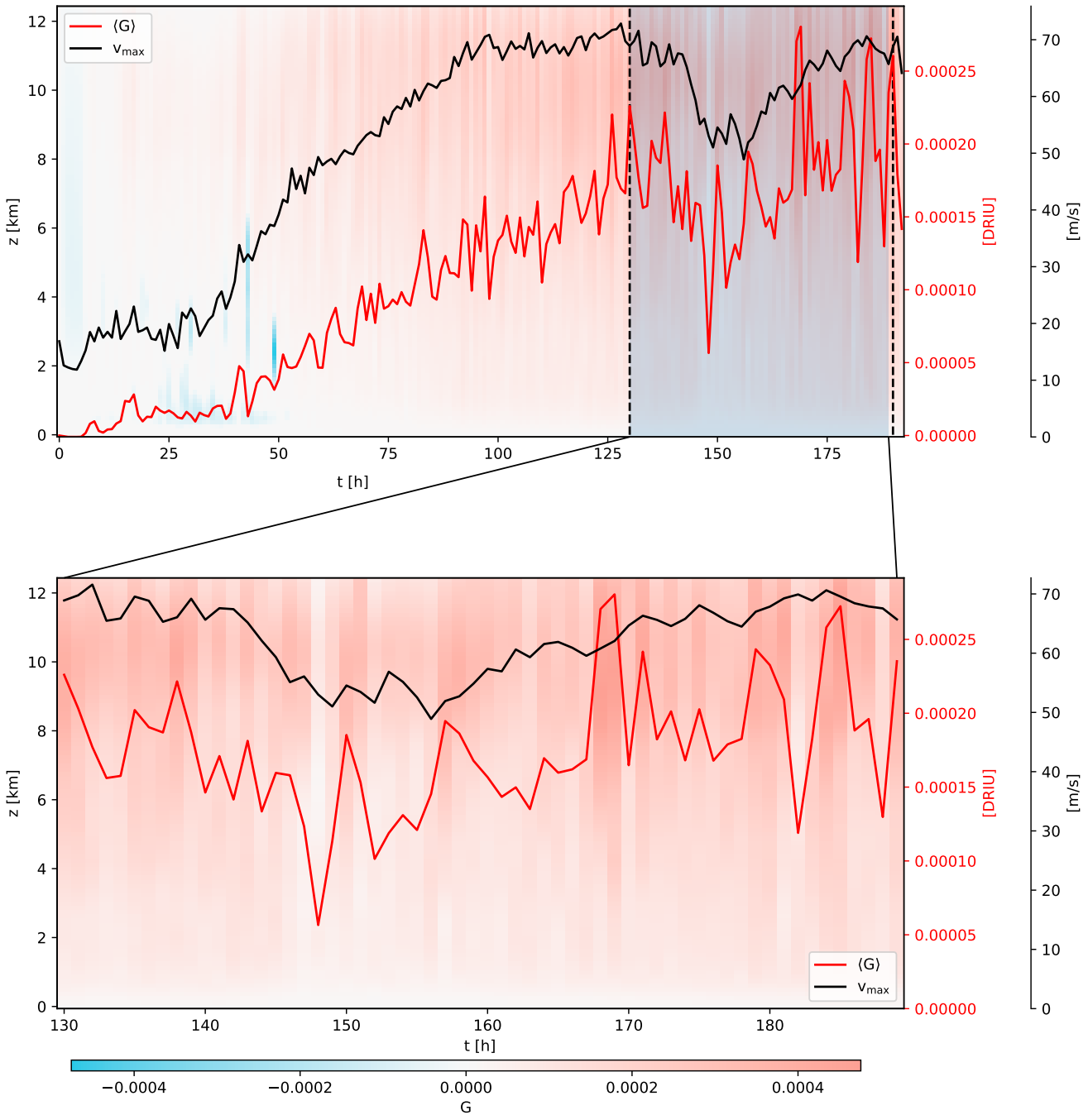

Figure 6. Horizontal average of diabatic transfer G for a TC in a slightly sheared environment shown in color-code. Analogously to fig. 2, the black curve indicates the maximum velocity of the storm, and the red curve the volume average of G through the whole depth of the atmosphere, both with axes to the right in the same color. The upper panel shows the full time series, and the lower panel focuses on the weakening and re-intensification phase between 130 and 180 h.

https://doi.org/10.5194/egusphere-2026-2918
Preprint. Discussion started: 11 June 2026

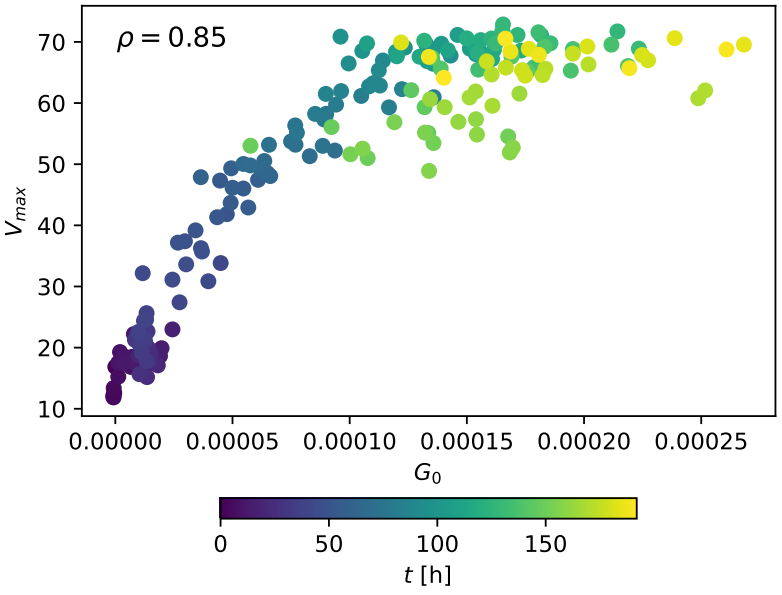

Figure 7. Scatter plot of correlation between G_0 and $v_{\max}$ for the idealized TC. The color code indicates the time evolution of the values and the Spearman's correlation coefficient is given by ρ.

While the evolution of Fourier-mode-0 energy transfer appears to be tightly connected to the intensity of the storm in that its evolution follows that of the maximum wind speed, changes in the Fourier-mode-1 energy transfer actually precedes intensity changes by about 3 h. Here, and in more detail in Dörffel et al. (2021), we argue that it is the perturbation of potential temperature that opens a pathway for diabatic heating to couple to the storm's energy balance (cf. eq. (5)). The potential temperature perturbations are the result of two processes, namely the balanced primary circulation developing a warm core and the tilt-induced dipolar modulation (Dörffel et al., 2021; Dörffel, 2022). Diabatic heating can couple to these modulations leading to negative bursts of Fourier-mode-1 energy transfer. That may negatively impact the intensity of the storm. In case of the storm presented here, however, we summarize that throughout most of the storm's development lower to mid-level Fourier-mode-1 kinetic energy transfer is mostly neutral with episodes of marginal negative impact.

For a more qualitative statement, however, we need to further analyze suitable cases that exhibit the necessary features. In particular, (synthetic) storm with a more enhanced tilt would allow to pinpoint the role of the Fourier-mode-1 component of diabatic heating. Producing this data would exceed the scope of the present study and is relayed to a future publication.

4.2 Florence case study

In the previous section, we analyzed an idealized setting of a TC. Since real-world cases are potentially more complex, in this section we analyze the three-dimensional organization of energy transfers for the Hurricane Florence (2018) case study using

https://doi.org/10.5194/egusphere-2026-2918
Preprint. Discussion started: 11 June 2026

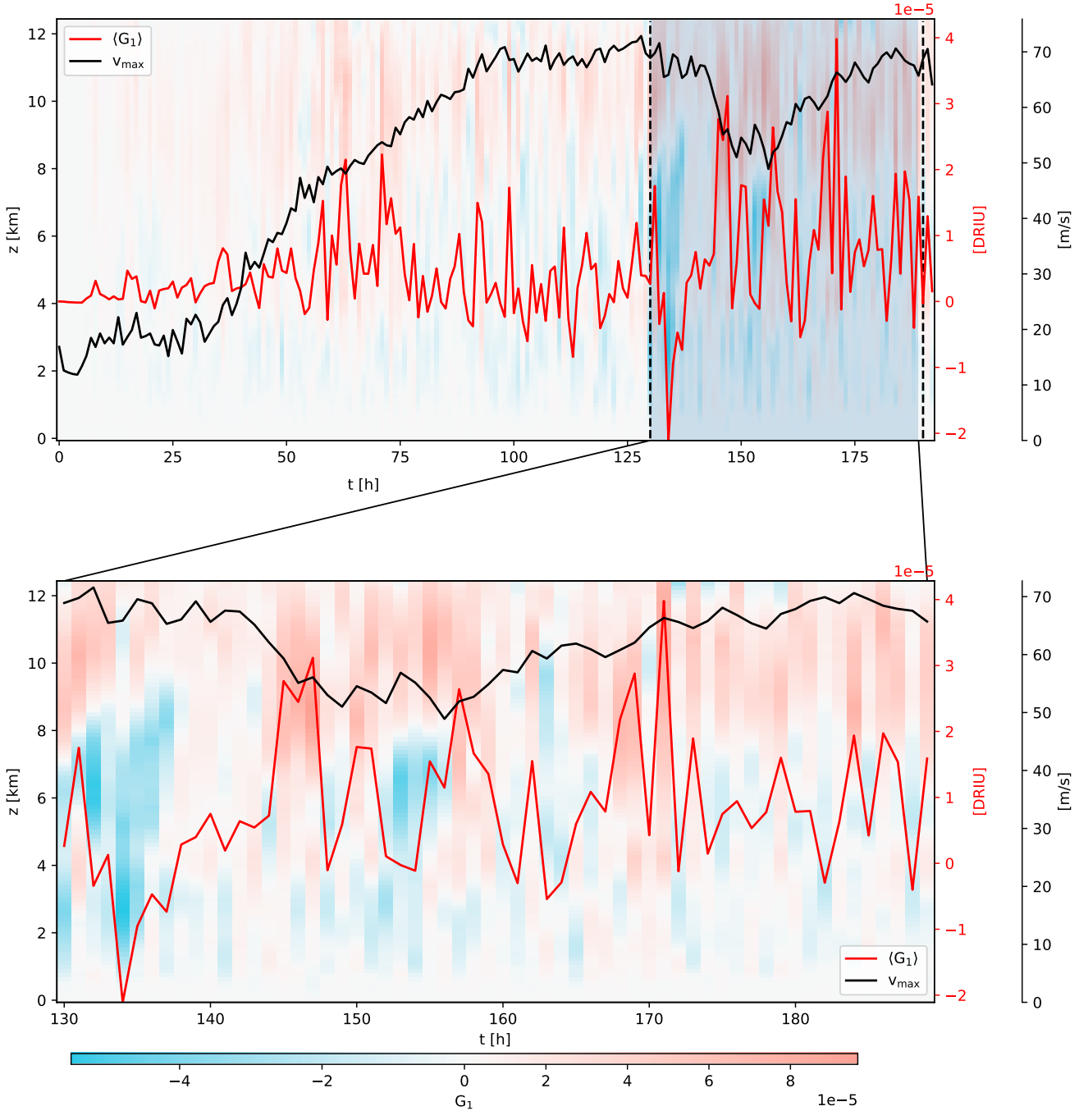

Figure 8. Same as fig. 6, but for the diabatic transfer G_1.

https://doi.org/10.5194/egusphere-2026-2918
Preprint. Discussion started: 11 June 2026

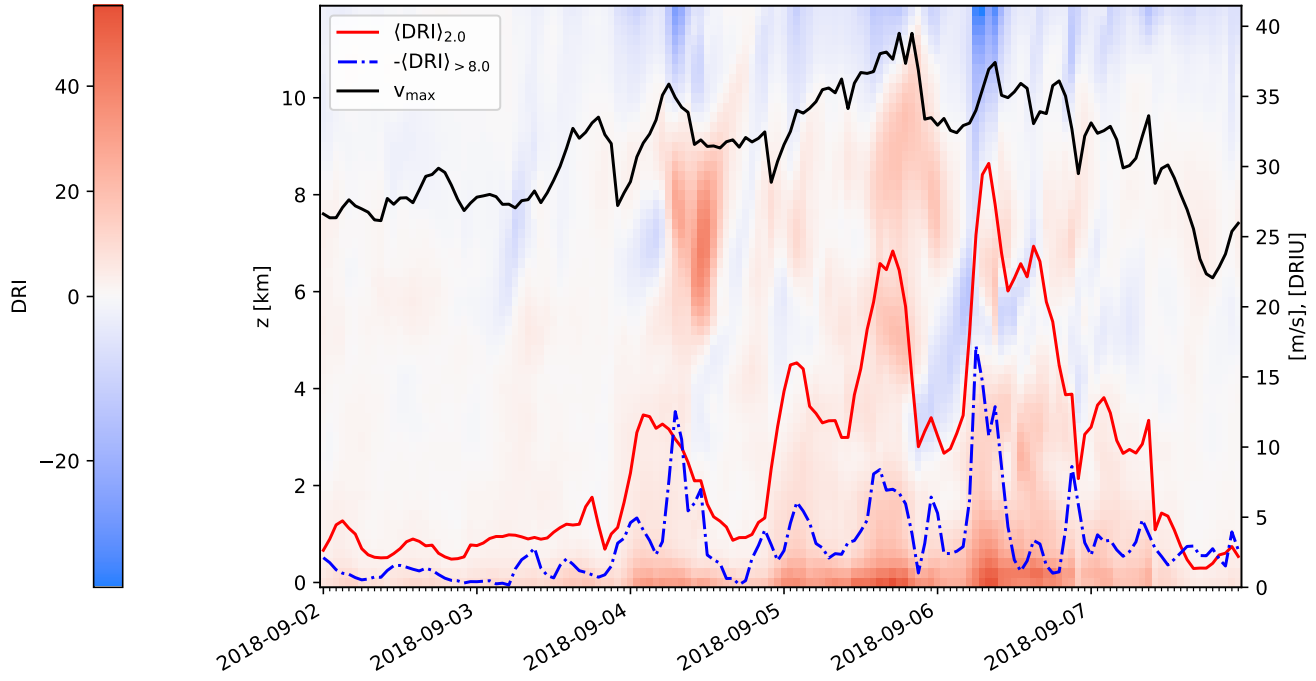

Figure 9. Evolution of the inertial energy transfers based on ERA5 data for 30 km scale length. Colors, lines and axes are described in fig. 2.

ERA5 reanalysis data. In analogy to the idealized setup, we therefore compute the inertial energy transfers as evaluated by the DRI (eq. (7)), along with the rates of generation of APE and conversion to KE (cf. eq. (5)).

Compared to the idealized case, we observe a more complex pattern of DRI throughout the atmosphere. In fig. 9 there are several episodes of intensification and attenuation that are accompanied by fluctuations in the DRI and diabatic transfer. Furthermore, there is less of a clear distinction of the boundary layer. Nevertheless, the qualitative behavior exhibits similarities to the idealized case. In particular, there are positive DRI values in a boundary layer near ocean surface, negative values at the top of the TC (above 10 km), and positive as well as negative values in the mid-troposphere. The magnitude of the vertical integrals of DRI up to $2\,\mathrm{km}$, filtered by DRI values > 0, correlates with the maximum wind speed ($\rho = 0.85$, see fig. 10). Similarly to the idealized case study, we observe smaller amplitudes of positive DRI values in the boundary layer during weakening phases of hurricane Florence, *i.e.*, at the second half of Sep 4 and around Sep 6, and higher DRI values in the intensification stages, e.g., midday of Sep 6. This indicates stronger downscale transfers, *i.e.*, convergence in the boundary layer close to the ocean surface during intense phases of the TC. Moreover, the negative DRI signals at the upper troposphere are stronger during more intense phases of Hurricane Florence and weaken during less intense phases.

The Fourier modes 0 and 1 of the diabatic transfer exhibit similar patterns to those observed in the idealized TC case. Higher (lower) positive values of Fourier mode 0 are present during the more (less) intense phases (fig. 11, top panel). The

https://doi.org/10.5194/egusphere-2026-2918
Preprint. Discussion started: 11 June 2026

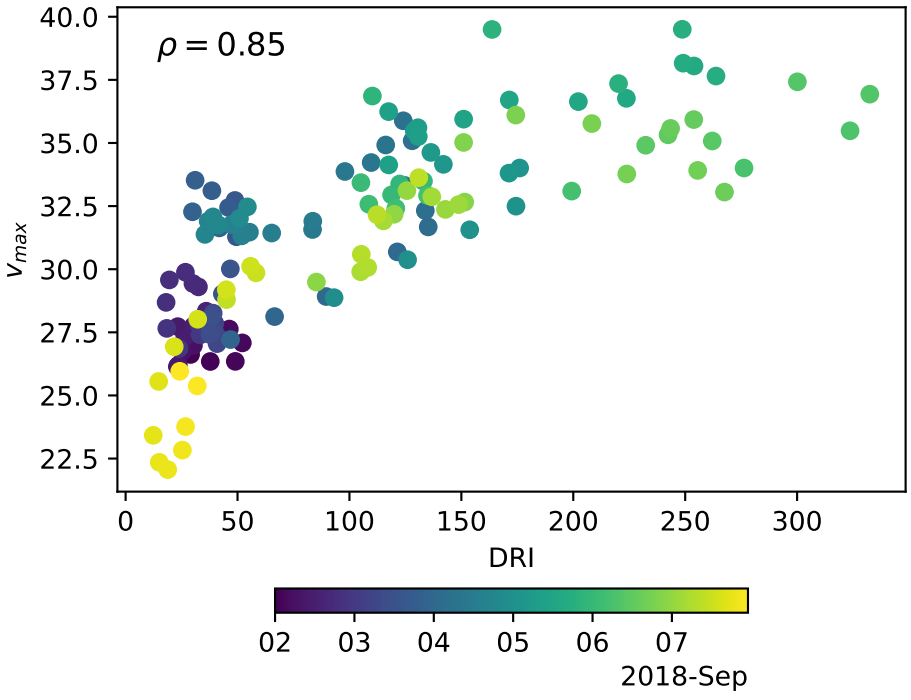

Figure 10. Correlation of intensity and inertial energy transfer for hurricane Florence (2018). The color code indicates the time evolution of the values and the Spearman's correlation coefficient is given by ρ.

365 correlation between the intensity and the Fourier-mode 0 of the diabatic transfer is significant (see fig. 12), although with a lower correlation coefficient ($\rho = 0.71$, $p < 0.05$).

The asymmetric contribution to the diabatic transfer (Fourier mode 1, fig. 11, bottom) is also in general agreement with the results of the idealized case: We observe mostly negative values in the lower troposphere below approximately $8\,\mathrm{km}$ and positive values above. There are several negative bursts that are in temporal proximity to episodes of attenuation. A clear 370 correlation however, cannot be established most likely due to the quality of the coarsely resolved data and the complexity of the real-world case. Future work must consider high-resolution data to further investigate the role of the Fourier mode 1 of the diabatic transfer in the context of TCs.

5 Conclusions

This study presents a blueprint of two complementary approaches for analyzing inter-scale inertial and diabatic energy transfers 375 that impact intensity changes of TCs. To this end, two case studies have been deployed, one idealized simulation and ERA5 reanalysis data of Hurricane Florence (2018). In the context of intensity changes, the structural organization of the energy pathways is examined. Characteristic features in the spatio-temporal fields of energy transfers have been found.

https://doi.org/10.5194/egusphere-2026-2918
Preprint. Discussion started: 11 June 2026

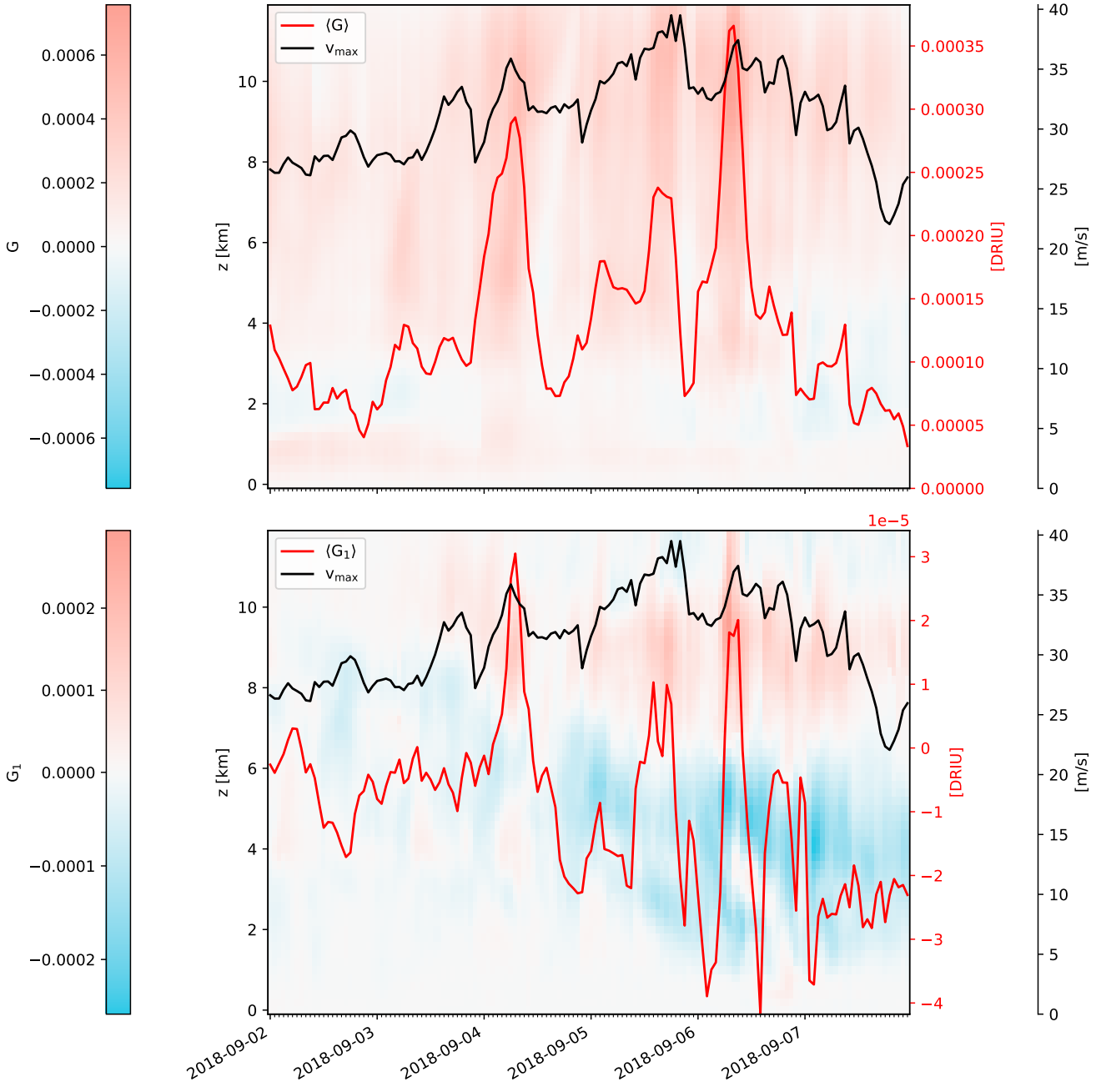

Figure 11. Time Evolution of the diabatic transfer G (top) and separately its Fourier mode 1 (bottom). Colors, lines and axes are described in fig. 6.

https://doi.org/10.5194/egusphere-2026-2918
Preprint. Discussion started: 11 June 2026

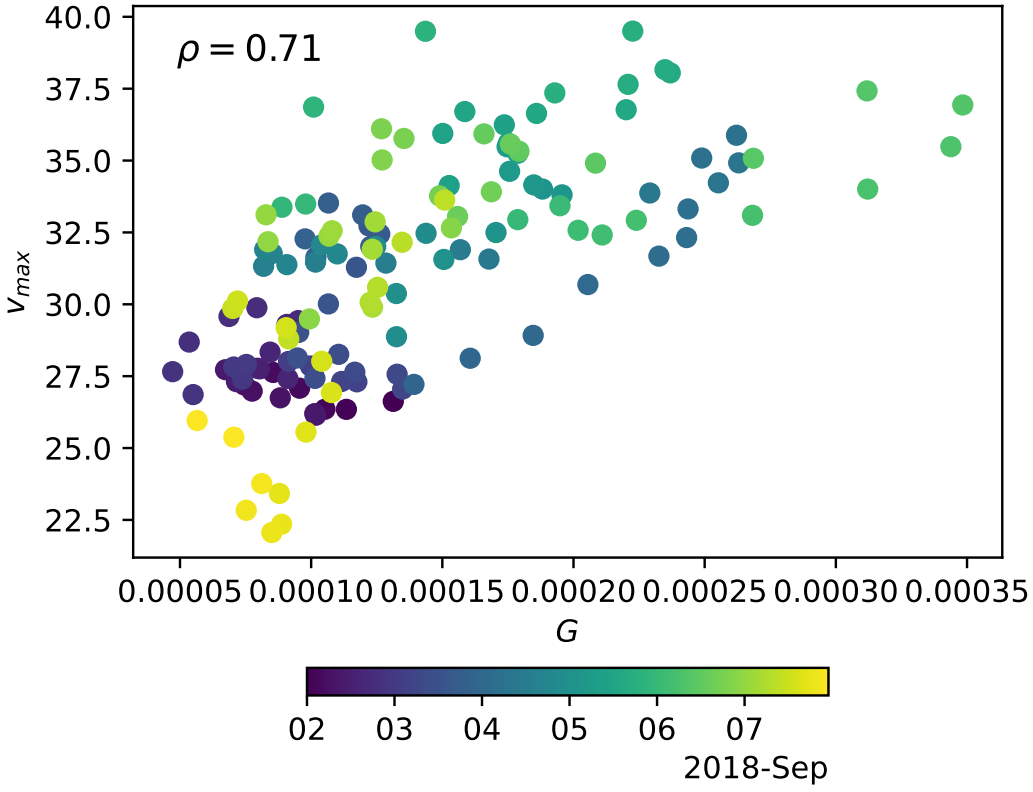

Figure 12. Correlation of intensity and the symmetric component of diabatic transfer G_0 for hurricane Florence (2018). The color code indicates the time evolution of the values and the Spearman's correlation coefficient is given by ρ.

The Duchon-Robert index (DRI) (Duchon and Robert, 2000b) is addressing the inter-scale transport of kinetic energy by accounting for contracting (expanding) energy fluxes through control volumes of a given scale size if the sign is positive (negative). The length scale at which analyses have been carried out on is $30\,\mathrm{km}$, *i.e.*, on a scale that is far above the turbulent mixing scale but just below the characteristic scale of the vortex core. Here, we focus on the inter-scale transport that accounts for injection (depletion) of kinetic energy onto (from) the storm's core scale by tapping kinetic energy from larger scales.

The flow organizes as follows: a prominent inflow establishes in the boundary layer close to the ocean surface, while mass conservation forces fluid parcels to move aloft and outwards. This is reflected in the organization of the DRI at peak intensity. At that stage, pronounced layers of positive DRI form closest to the ocean surface. Intensity correlates with the amplitude of the boundary layer inflow, *i.e.*, the DRI in the boundary layer (cf. fig. 2). While phases of intensification are accompanied by an uptake of the boundary layer inflow, the idealized simulation showed that the deterioration of the boundary layer energy convergence correlates with the weakening of the storm.

With this study, we emphasize the geometric structure of these transfers and found that the DRI patterns organize along the tilted centerline for all sets of data throughout all phases of storm development. While the DRI indicates mostly symmetric

https://doi.org/10.5194/egusphere-2026-2918
Preprint. Discussion started: 11 June 2026

radial inflow in the boundary layer and radial outflow on top of the storm, the middle layers consistently exhibit pronounced dipolar structures throughout most of the depth of the troposphere (cf. fig. 4). These structures are clearly aligned along the tilted centerline. It is evident that these patterns reflect contraction or expansions of kinetic energy. A possible interpretation of these structures may be found through mass continuity. Vertical motions, either self-induced through the centerline tilt (Dörffel et al., 2021) or the result of heat release, are accompanied by convergent/divergent compensating flows, depending on the sign of vertical momentum transport. For a profound physical interpretation, however, it is necessary to perform further analyses on more diverse sets of data to assess whether these structures are universal to TCs.

As being a purely kinematic measure[2], the DRI approach on the one hand does not account for sources of energy that causes intensification/weakening. In fact, most of the energy a TC needs to establish and maintain the primary circulation is harvested from deep convective processes in the troposphere (Houze, 2010). Deep-convection, again, drives mass and momentum transport as a multiscale phenomenon where the motions of air masses of individual small-scale cloud towers accumulate to establish the secondary circulation on a larger scale (Montgomery and Smith, 2017b). It is believed that it is entrainment in a shallow layer just above the frictional boundary layer that causes for the angular momentum transport necessary to intensify the storm (Smith and Montgomery, 2024; Dörffel et al., 2026).

For both, the DRI and diabatic transfer approaches, we observe that the structure organize along the tilted centerline. For the diabatic transfer approach, this is not surprising, as the method is constructed around the notion of a centerline as the position of the center of rotation per height level. Nonetheless, the insights gained through the diabatic transfer analyses and the interpretation of the results are reasonable with respect to the asymptotic theory (Päschke et al., 2012) even though both cases did not provide substantial tilts. Future studies need to focus on case studies providing substantial tilt. For the DRI approach, however, we see similarly structures aligning along the centerline. We therefore conclude, that these structures, mostly symmetric in the boundary layer, and mostly dipolar in the bulk of the vortex, are related to the structure and the dynamics of the TC. A more detailed discussion of the physical interpretation of the DRI fields, however, is out-of-scope of the present study due to a limited data quality and resolution as well as the fact, that we have restricted our analysis to a scale length of $30\,\mathrm{km}$ and therefore left to future research.

We conclude that the presented analysis opens a promising route towards understanding and predicting TC intensity changes on the basis of energy budgets. For all the presented test cases clear signals preceded or correlated with these events of interest. Bhalachandran et al. (2020) claims that there is a need for a "more sophisticated framework [...] to describe the various energy interactions". In contrast to the analysis based on the spectral composition of the data, we here propose a novel approach that is motivated by the physical properties of the storm dynamics, yet related to existing methods based on the APE theory of Lorenz (1955). The complementary signals in the DRI and the diabatic transfer are constructed along the (symmetric and asymmetric) fluid-dynamical and thermodynamical properties and account for insights into the scale- and energetic interactions of the flow structure. Potentially, from the combination of both flavors of energy transfer, general-purpose indicators might be constructed that can be used for signaling and predicting RI/RW events ultimately performing as risk indicators.

[2]The DRI is a measure for the in-/outflow of kinetic energy through a control volume.

https://doi.org/10.5194/egusphere-2026-2918
Preprint. Discussion started: 11 June 2026

Although the presented study delivered promising results, we need to mention its limitations related to the quality of the data. Although Hurricane Florence (2018) did undergo several phases of rapid intensification and weakening, the ERA5 data does not fully represent the true historic development of the storm. We see, however, indications in terms of DRI and diabatic transfer that potentially could have lead to intensity changes if the model dynamics had allowed for it. A systematic assessment of high-resolution forecast data together with reanalysis data would let us draw conclusions on whether and how the two indicator can be used for predicting RI/RW events even for under-resolved data. Here, for the sake of focusing on the theoretical background and illustrating the basic concepts, however, we did not apply the methods to a broader catalogue of interesting test cases. Of particular interest is the question of how universal our findings apply to TCs. To this end, an extended analysis across various data sources (*e.g.*, Judt, 2018; Leighton et al., 2018, among others) and ocean basins is proposed. This will be subject to future research.

Code and data availability. The data for Hurricane Florence's best estimate track can be accessed through the database HURDAT2 of the National Oceanic and Atmospheric Administration (NOAA): https://www.aoml.noaa.gov/hrd/hurdat/hurdat2.html. The ERA5 reanalysis (Hersbach et al., 2020) is provided by the European Center for Medium-Range Weather Forecasts (ECMWF) and can be downloaded from the Copernicus Climate Change Service (C3S) Climate Date Store. Data produced by CM1 has been made available on a public data server (Dörffel et al., 2025). The data analysis has been conducted with modules implemented into the proprietary research software Amira and thus cannot be published along with this work. Similar analysis, however, can be conducted with the open-source package LoSSETT (https://github.com/ElliotMG/LoSSETT/tree/master).

Appendix A: Diabatic transfer analysis

The asymptotic model of Päschke et al. (2012) and the analytical findings of Dörffel et al. (2021) motivated introducing the notion of a centerline and perform an azimuthal wavenumber in a tilted cylindrical system. The leading-order equations of the asymptotic bulk-vortex model (see Päschke et al. (2012); Dörffel et al. (2021)) reveal the interaction of the azimuthally mean flow with symmetric and wavenumber-1 diabatic heat release. Details of the energy-budget equations are given in appendix A. From a physical point of view, this is due to the tilted structure of the vortex that induces wavenumber-1 modulations of the thermodynamic fields in the balanced vortex, which in turn open pathways to energy exchanges of the leading-order flow structure with diabatic heating (Dörffel et al., 2021). Here, we want to summarize the energy pathways that may lead to intensity changes and highlight the role of the symmetric and asymmetric contributions.

The dominant flow component is the tangential velocity u_θ, all the other contributions are — asymptotically speaking — of higher order and can thus be neglected in the energy budget. Hence, the resulting kinetic energy equation in cylindrical coordinates (cf. fig. A1) reads

$$\frac{\partial e_{\text{kin}}}{\partial t} + \frac{1}{r}\frac{\partial}{\partial r}\left(r u_{r,00} h_{\text{kin}}\right) + \frac{\partial}{\partial z}\left(w_0 h_{\text{kin}}\right) = g\rho w \frac{\Theta'}{\Theta} + \text{h.o.t.} \tag{A1}$$

https://doi.org/10.5194/egusphere-2026-2918
Preprint. Discussion started: 11 June 2026

with the definitions of the kinetic energy density

$$e_{\text{kin}} = \frac{1}{2}\rho|\boldsymbol{u}|^2 = \frac{1}{2}\rho u_\theta^2 + \text{h.o.t.} \tag{A2}$$

and

$$h_{\text{kin}} = e_{\text{kin}} + p\,. \tag{A3}$$

r, θ, and z are quasi-cylindrical coordinates (radius, azimuth, and height, resp.) with respect to the coordinate system attached to the tilted centerline, and t is time.

In his seminal work, Lorenz (1955) budgeted the energy transition between diabatic heating, the mean-field atmospheric available potential (APE) and kinetic energy (KE) by

$$\frac{d\bar{A}}{dt} = G - C\,, \tag{A4}$$
$$\frac{d\bar{K}}{dt} = C - D\,, \tag{A5}$$

with $\bar{A}$ being the mean APE, $\bar{K}$ the mean KE, G the generation rate of APE, C the conversion of APE to KE, and D the frictional dissipation. For an isolated TC, Dörffel et al. (2021) found the following expression for G and C:

$$G = \int_V \frac{g\rho}{\partial_z \Theta} \frac{\Theta' Q'_\Theta}{\Theta}\, dV + \text{h.o.t.} \tag{A6}$$
$$C = -\frac{1}{|A|}\int_V \boldsymbol{u}\cdot\nabla_{\|} p\, dV + \text{h.o.t.} \tag{A7}$$

At leading order, the amount of generated APE equals the rate at which APE is converted to kinetic energy:

$$G \approx \int_V g\rho\frac{\Theta' w}{\Theta}\, dV \approx C \tag{A8}$$

The transition is the result of the correlation of the potential temperature perturbation Θ' and vertical velocity w, where the latter is the result of both, diabatic heating and adiabatic lift due to the tilted structure of the storm (Frank and Ritchie, 1999; Päschke et al., 2012; Dörffel et al., 2021). In centerline-relative coordinates, we can decompose eq. (A8) into the symmetric and asymmetric contribution leading to eq. (5).

Competing interests. The authors declare no competing interests.

https://doi.org/10.5194/egusphere-2026-2918
Preprint. Discussion started: 11 June 2026

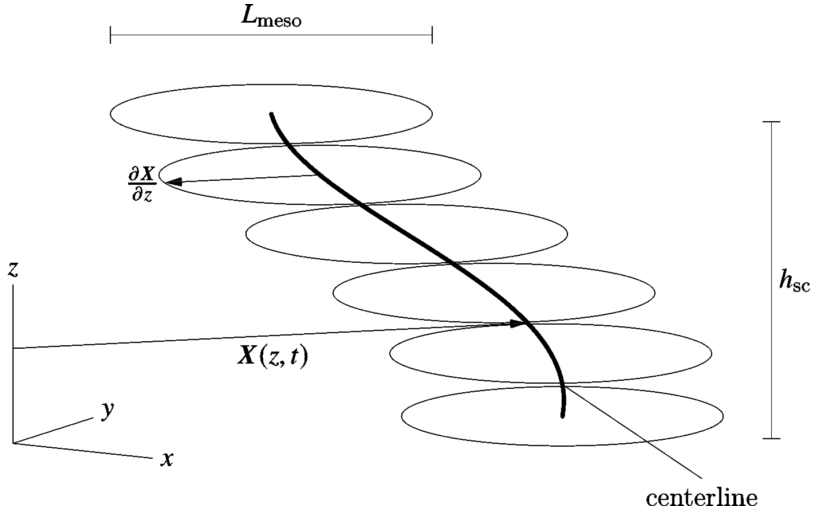

Figure A1. Schematic flow structure of idealized TC. Shown is the symmetric primary flow structure aligned along a tilted centerline with time and height-dependent position $\boldsymbol{X}(z,t)$. Adapted from Päschke et al. (2012)

Acknowledgements. The authors acknowledge funding by the Deutsche Forschungsgemeinschaft (DFG) Collaborative Research Center CRC1114, "Scaling Cascades in Complex system" through the projects C06 and B07. The international scientific exchanges were greatly facilitated by funding through the DAAD exchange program Procope Plus through the project "Energetics and drivers of extreme convective events". The authors would like to thank the HPC Service of ZEDAT, Freie Universität Berlin (HPC system Curta, see Bennett et al., 2020, for details), for providing computational resources.

https://doi.org/10.5194/egusphere-2026-2918
Preprint. Discussion started: 11 June 2026

References

Aluie, H., Hecht, M., and Vallis, G. K.: Mapping the Energy Cascade in the North Atlantic Ocean: The Coarse-Graining Approach, Journal of Physical Oceanography, 48, 225–244, 2018.

Alvey, III, G. R., Zawislak, J., and Zipser, E.: Precipitation Properties Observed during Tropical Cyclone Intensity Change, Monthly Weather Review, 143, 4476–4492, https://doi.org/10.1175/MWR-D-15-0065.1, 2015.

Bennett, L., Melchers, B., and Proppe, B.: Curta: A General-purpose High-Performance Computer at ZEDAT, Freie Universität Berlin, http://dx.doi.org/10.17169/refubium-26754, 2020.

Bhalachandran, S., Chavas, D. R., Jr, F. D. M., Dubey, S., Shreevastava, A., and Krishnamurti, T. N.: Characterizing the Energetics of Vortex-Scale and Sub-Vortex-Scale Asymmetries during Tropical Cyclone Rapid Intensity Changes, Journal of the Atmospheric Sciences, 77, 315–336, https://doi.org/10.1175/JAS-D-19-0067.1, publisher: American Meteorological Society Section: Journal of the Atmospheric Sciences, 2020.

Bryan, G. H.: Effects of Surface Exchange Coefficients and Turbulence Length Scales on the Intensity and Structure of Numerically Simulated Hurricanes, Monthly Weather Review, 140, 1125 – 1143, https://doi.org/10.1175/MWR-D-11-00231.1, 2012.

Bryan, G. H. and Fritsch, J. M.: A benchmark simulation for moist nonhydrostatic numerical models, Monthly Weather Review, 130, 2917–2928, 2002.

Byrne, D. and Zhang, J. A.: Height-dependent transition from 3-D to 2-D turbulence in the hurricane boundary layer, Geophysical Research Letters, 40, 1439–1442, 2013.

Callaghan, J.: Asymmetric Inner Core Convection Leading to Tropical Cyclone Intensification, Tropical Cyclone Research and Review, 6, 55–66, https://doi.org/10.6057/2017TCRRh3.02, 2017.

Dubrulle, B.: Beyond Kolmogorov cascades, Journal of Fluid Mechanics, 867, https://hal.archives-ouvertes.fr/hal-02056504/document, 2019.

Duchon, J. and Robert, R.: Inertial energy dissipation for weak solutions of incompressible Euler and Navier-Stokes equations, Nonlinearity, 13, 249, 2000a.

Duchon, J. and Robert, R.: Inertial energy dissipation for weak solutions of incompressible Euler and Navier-Stokes equations, Nonlinearity, 13, 249, https://doi.org/10.1088/0951-7715/13/1/312, publisher: IOP Publishing, 2000b.

Dunion, J. P.: Rewriting the climatology of the tropical North Atlantic and Caribbean Sea atmosphere, Journal of Climate, 24, 893–908, 2011.

Dunkerton, T. J., Montgomery, M. T., and Wang, Z.: Tropical Cyclogenesis in a Tropical Wave Critical Layer: Easterly Waves, Atmos. Chem. Phys., p. 60, 2009.

Dörffel, T.: Moisture-Induced Dynamics of Tilted Tropical Cyclones, Ph.D. thesis, Freie Universität Berlin, Berlin, http://dx.doi.org/10.17169/refubium-41065, accepted: 2023-10-30T13:27:48Z, 2022.

Dörffel, T., Papke, A., Klein, R., Ernst, N., and Smolarkiewicz, P. K.: Dynamics of tilted atmospheric vortices under asymmetric diabatic heating, Theoretical and Computational Fluid Dynamics, 35, 831–873, 2021.

Dörffel, T., Mikula, N., Schielicke, L., Kiszler, T., Faranda, D., Debrulle, B., and Vercauteren, N.: Characterizing inertial and diabatic energy transfers in tropical cyclones: Data, https://doi.org/10.12752/10135, 2025.

Dörffel, T., Doppler, S., Khouider, B., and Klein, R.: Intensification of a tropical cyclone: Triple-deck theoriy for the control of convection, to be submitted, 2026.

https://doi.org/10.5194/egusphere-2026-2918
Preprint. Discussion started: 11 June 2026

Faranda, D., Lembo, V., Iyer, M., Kuzzay, D., Chibbaro, S., Daviaud, F., and Dubrulle, B.: Computation and Characterization of Local Subfilter-Scale Energy Transfers in Atmospheric Flows, Journal of the Atmospheric Sciences, 75, 2175–2186, https://doi.org/10.1175/JAS-D-17-0114.1, publisher: American Meteorological Society Section: Journal of the Atmospheric Sciences, 2018.

Frank, W. M. and Ritchie, E. A.: Effects of Environmental Flow upon Tropical Cyclone Structure, Monthly Weather Review, 127, 2044–2061, 1999.

Germano, M.: Turbulence: the filtering approach, Journal of Fluid Mechanics, 238, 325–336, https://doi.org/10.1017/S0022112092001733, 1992.

Gregory, D.: The Mass-Flux Approach to the Parametrization of Deep Convection March 1997, 2002.

Grinsted, A., Ditlevsen, P., and Christensen, J. H.: Normalized US hurricane damage estimates using area of total destruction, 1900- 2018, Proceedings of the National Academy of Sciences, 116, 23 942–23 946, 2019.

Hendricks, E. A., Montgomery, M. T., and Davis, C. A.: The Role of "Vortical" Hot Towers in the Formation of Tropical Cyclone Diana (1984), Journal of the Atmospheric Sciences, 61, 1209 – 1232, https://doi.org/10.1175/1520-0469(2004)061<1209:TROVHT>2.0.CO;2, 2004.

Hersbach, H., Bell, B., Berrisford, P., Hirahara, S., Horányi, A., Muñoz-Sabater, J., Nicolas, J., Peubey, C., Radu, R., Schepers, D., et al.: The ERA5 global reanalysis, Quarterly Journal of the Royal Meteorological Society, 146, 1999–2049, 2020.

Hodges, K., Cobb, A., and Vidale, P. L.: How Well Are Tropical Cyclones Represented in Reanalysis Datasets?, Journal of Climate, 30, 5243 – 5264, https://doi.org/10.1175/JCLI-D-16-0557.1, 2017.

Houze, R. A.: Clouds in Tropical Cyclones, Monthly Weather Review, 138, 293–344, https://doi.org/10.1175/2009MWR2989.1, 2010.

Hunt, J. C., Wray, A. A., and Moin, P.: Eddies, streams, and convergence zones in turbulent flows, Studying turbulence using numerical simulation databases, 2. Proceedings of the 1988 summer program, available at https://ntrs.nasa.gov/api/citations/19890015184/downloads/19890015184.pdf, 1988.

IPCC: IPCC 2021: Climate Change 2021: The Physical Science Basis. Contribution of Working Group I to the Sixth Assessment Report of the Intergovernmental Panel on Climate Change, Tech. rep., IPCC, 2021.

Judt, F.: Insights into Atmospheric Predictability through Global Convection-Permitting Model Simulations, Journal of the Atmospheric Sciences, 75, 1477–1497, https://doi.org/10.1175/JAS-D-17-0343.1, publisher: American Meteorological Society Section: Journal of the Atmospheric Sciences, 2018.

Klein, R.: Scale-Dependent Models for Atmospheric Flows, Annual Review of Fluid Mechanics, 42, 249–274, https://doi.org/10.1146/annurev-fluid-121108-145537, 2010.

Kossin, J., Hall, T., Knutson, T., Kunkel, K., Trapp, R., Waliser, D., and Wehner, M.: Extreme storms, 2017.

Kuzzay, D., Faranda, D., and Dubrulle, B.: Global vs local energy dissipation: The energy cycle of the turbulent von Kármán flow, Physics of Fluids (1994-present), 27, 075 105, 2015.

Kuzzay, D., Saw, E. W., J W A Martins, F., Faranda, D., Foucaut, J.-M., Daviaud, F., and Dubrulle, B.: New method for detecting singularities in experimental incompressible flows, Nonlinearity, 30, 2381–2402, https://doi.org/10.1088/1361-6544/aa6aaf, 2017.

Ladwig, W.: Wrf-Python, UCAR/NCAR, 2017.

Landsea, C. W. and Franklin, J. L.: Atlantic hurricane database uncertainty and presentation of a new database format, Monthly Weather Review, 141, 3576–3592, 2013.

https://doi.org/10.5194/egusphere-2026-2918
Preprint. Discussion started: 11 June 2026

Leighton, H., Gopalakrishnan, S., Zhang, J. A., Rogers, R. F., Zhang, Z., and Tallapragada, V.: Azimuthal Distribution of Deep Convection, Environmental Factors, and Tropical Cyclone Rapid Intensification: A Perspective from HWRF Ensemble Forecasts of Hurricane Edouard (2014), Journal of the Atmospheric Sciences, 75, 275–295, https://doi.org/10.1175/JAS-D-17-0171.1, 2018.

Leonard, A.: Energy Cascade in Large-Eddy Simulations of Turbulent Fluid Flows, in: Advances in Geophysics, edited by Frenkiel, F. N. and Munn, R. E., vol. 18 of *Turbulent Diffusion in Environmental Pollution*, pp. 237–248, Elsevier, https://doi.org/10.1016/S0065-2687(08)60464-1, 1975.

Li, Q. and Dai, Y.: Revisiting Azimuthally Asymmetric Moist Instability in the Outer Core of Sheared Tropical Cyclones, Monthly Weather Review, 148, 1297–1319, https://doi.org/10.1175/MWR-D-19-0004.1, 2019.

Lorenz, E. N.: Available Potential Energy and the Maintenance of the General Circulation, Tellus, 7, 157–167, 1955.

Marks, F. D., Houze Jr., R. A., and Gamache, J. F.: Dual-Aircraft Investigation of the Inner Core of Hurricane Norbert. Part I: Kinematic Structure, Journal of the Atmospheric Sciences, 49, 919–942, https://doi.org/10.1175/1520-0469(1992)049<0919:DAIOTI>2.0.CO;2, 1992.

Marks, F. D., Black, P. G., Montgomery, M. T., and Burpee, R. W.: Structure of the Eye and Eyewall of Hurricane Hugo (1989), Monthly Weather Review, 136, 1237–1259, https://doi.org/10.1175/2007MWR2073.1, 2008.

Meneveau, C.: Statistics of Turbulence Subgrid-Scale Stresses - Necessary Conditions and Experimental Tests, in: Physics of Fluids, pp. 815–833, http://gateway.webofknowledge.com/gateway/Gateway.cgi?GWVersion=2&SrcAuth=mekentosj&SrcApp=Papers&DestLinkType=FullRecord&DestApp=WOS&KeyUT=A1994NA73900014, 1994.

Mikula, N., Dörffel, T., Baum, D., and Hege, H.-C.: An Interactive Approach for Identifying Structure Definitions, Computer Graphics Forum, 41, 321–332, https://doi.org/10.1111/cgf.14543, 2022.

Montgomery, M. T. and Smith, R. K.: On the Applicability of Linear, Axisymmetric Dynamics in Intensifying and Mature Tropical Cyclones, Fluids, 2, 69, https://doi.org/10.3390/fluids2040069, 2017a.

Montgomery, M. T. and Smith, R. K.: Recent Developments in the Fluid Dynamics of Tropical Cyclones, Annual Review of Fluid Mechanics, 49, 541–574, https://doi.org/10.1146/annurev-fluid-010816-060022, 2017b.

Montgomery, M. T., Nicholls, M. E., Cram, T. A., and Saunders, A. B.: A Vortical Hot Tower Route to Tropical Cyclogenesis, Journal of the Atmospheric Sciences, 63, 355 – 386, https://doi.org/10.1175/JAS3604.1, 2006.

Munich Re: Hurricanes, typhoons, cyclones – Tropical storms: The natural hazard with the highest losses, https://www.munichre.com/en/risks/natural-disasters/hurricanes.html, (last access: 15-Feb-2024), 2024.

Nguyen, L. T., Molinari, J., and Thomas, D.: Evaluation of Tropical Cyclone Center Identification Methods in Numerical Models, Mon. Weather Rev., 142, 4326 – 4339, https://doi.org/10.1175/MWR-D-14-00044.1, 2014.

Nolan, D. S. and Grasso, L. D.: Nonhydrostatic, Three-Dimensional Perturbations to Balanced, Hurricane-Like Vortices. Part II: Symmetric Response and Nonlinear Simulations, JOURNAL OF THE ATMOSPHERIC SCIENCES, 60, 29, 2003.

Nolan, D. S. and Montgomery, M. T.: Nonhydrostatic, Three-Dimensional Perturbations to Balanced, Hurricane-like Vortices. Part I: Linearized Formulation, Stability, and Evolution, JOURNAL OF THE ATMOSPHERIC SCIENCES, 59, 32, 2002.

Paterson, L. A., Hanstrum, B. N., Davidson, N. E., and Weber, H. C.: Influence of environmental vertical wind shear on the intensity of hurricane-strength tropical cyclones in the Australian region, Monthly Weather Review, 133, 3644–3660, 2005.

Pauluis, O. M. and Zhang, F.: Reconstruction of Thermodynamic Cycles in a High-Resolution Simulation of a Hurricane, Journal of the Atmospheric Sciences, 74, 3367–3381, https://doi.org/10.1175/JAS-D-16-0353.1, 2017.

https://doi.org/10.5194/egusphere-2026-2918
Preprint. Discussion started: 11 June 2026

Päschke, E., Marschalik, P., Owinoh, A. Z., and Klein, R.: Motion and structure of atmospheric mesoscale baroclinic vortices: dry air and weak environmental shear, Journal of Fluid Mechanics, 701, 137–170, https://doi.org/10.1017/jfm.2012.144, publisher: Cambridge University Press, 2012.

Reasor, P. D., Montgomery, M. T., Marks Jr., F. D., and Gamache, J. F.: Low-Wavenumber Structure and Evolution of the Hurricane Inner Core Observed by Airborne Dual-Doppler Radar, Monthly Weather Review, 128, 1653–1680, 2000.

Reasor, P. D., Montgomery, M. T., and Grasso, L. D.: A New Look at the Problem of Tropical Cyclones in Vertical Shear Flow: Vortex Resiliency, JOURNAL OF THE ATMOSPHERIC SCIENCES, 61, 20, 2004.

Riemer, M., Montgomery, M. T., and Nicholls, M. E.: A New Paradigm for Intensity Modification of Tropical Cyclones: Thermodynamic Impact of Vertical Wind Shear on the Inflow Layer, Atmos. Chem. Phys., p. 26, 2010.

Rios-Berrios, R.: Impacts of Radiation and Cold Pools on the Intensity and Vortex Tilt of Weak Tropical Cyclones Interacting with Vertical Wind Shear, Journal of Atmospheric Sciences, 77, 669–689, 2020.

Roberts, M. J., Camp, J., Seddon, J., Vidale, P. L., Hodges, K., Vannière, B., Mecking, J., Haarsma, R., Bellucci, A., Scoccimarro, E., et al.: Projected future changes in tropical cyclones using the CMIP6 HighResMIP multimodel ensemble, Geophysical Research Letters, 47, e2020GL088 662, 2020.

Rotunno, R. and Emanuel, K. A.: An Air–Sea Interaction Theory for Tropical Cyclones. Part II: Evolutionary Study Using a Nonhydrostatic Axisymmetric Numerical Model, Journal of the Atmospheric Sciences, 44, 542–561, https://doi.org/10.1175/1520-0469(1987)044<0542:AAITFT>2.0.CO;2, 1987.

Schecter, D. A.: Response of a Simulated Hurricane to Misalignment Forcing Compared to the Predictions of a Simple Theory, Journal of the Atmospheric Sciences, 72, 1235–1260, https://doi.org/10.1175/JAS-D-14-0149.1, 2015.

Schecter, D. A.: Intensification of Tilted Tropical Cyclones over Relatively Cool and Warm Oceans in Idealized Numerical Simulations, Journal of the Atmospheric Sciences, 79, 485–512, https://doi.org/10.1175/JAS-D-21-0051.1, 2022.

Schielicke, L., Névir, P., and Ulbrich, U.: Kinematic vorticity number–a tool for estimating vortex sizes and circulations, Tellus A: Dynamic Meteorology and Oceanography, 68, 29 464, 2016.

Schielicke, L., Gatzen, C. P., and Ludwig, P.: Vortex identification across different scales, Atmosphere, 10, 518, 2019.

Schielicke, L., Li, Y., Schyns, J., Sperschneider, A., Solano Marchini, J. P., and Gatzen, C. P.: Meeting summary: Exploring cloud dynamics with Cloud Model 1 and 3D visualization – insights from a university modeling workshop, Weather and Climate Dynamics, 5, 703–710, https://doi.org/10.5194/wcd-5-703-2024, 2024.

Shutts, G.: A kinetic energy backscatter algorithm for use in ensemble prediction systems, Quarterly Journal of the Royal Meteorological Society, 131, 3079–3102, https://doi.org/https://doi.org/10.1256/qj.04.106, 2005.

Simpson, R. H. and Saffir, H.: The hurricane disaster potential scale, Weatherwise, 27, 169, 1974.

Smith, A. B. and Katz, R. W.: US billion-dollar weather and climate disasters: data sources, trends, accuracy and biases, Natural hazards, 67, 387–410, 2013.

Smith, R. K. and Montgomery, M. T.: Can one reconcile the classical theories and the WISHE theories of tropical cyclone intensification?, TROPICAL CYCLONE RESEARCH REPORT, 150, 1–15, https://www.meteo.physik.uni-muenchen.de/~roger/Publications/M42B.pdf, 2024.

Spearman, C.: The Proof and Measurement of Association between Two Things, The American Journal of Psychology, 15, 72–101, https://doi.org/10.2307/1412159, 1904.

https://doi.org/10.5194/egusphere-2026-2918
Preprint. Discussion started: 11 June 2026

Sroka, S. and Guimond, S.: Organized Kinetic Energy Backscatter in the Hurricane Boundary Layer from Radar Measurements, Journal of Fluid Mechanics, 924, A21, https://doi.org/10.1017/jfm.2021.632, 2021.

Stewart, S. R. and Berg, R.: Hurricane Florence - Tropical Cyclone Report, resreport, National Hurricane Center, 2019.

Tang, J., Byrne, D., Zhang, J. A., Wang, Y., Lei, X.-t., Wu, D., Fang, P.-z., and Zhao, B.-k.: Horizontal Transition of Turbulent Cascade in the Near-Surface Layer of Tropical Cyclones, Journal of Atmospheric Sciences, 72, 4915–4925, 2015.

Tong, C., Wyngaard, J. C., and Brasseur, J.: Experimental study of the subgrid-scale stresses in the atmospheric surface layer, Journal of Atmospheric Sciences, 56, 2277–2292, http://journals.ametsoc.org/doi/abs/10.1175/1520-0469(1999)056%3C2277%3AESOTSS%3E2.0.CO%3B2, 1999.

Tory, K. J., Dare, R., Davidson, N., McBride, J., and Chand, S.: The importance of low-deformation vorticity in tropical cyclone formation, Atmospheric Chemistry and Physics, 13, 2115–2132, 2013.

Vannitsem, S. and Ghil, M.: Evidence of coupling in ocean-atmosphere dynamics over the North Atlantic, Geophysical Research Letters, 44, 2016–2026, 2017.

Vercauteren, N., Bou-Zeid, E., Parlange, M., Lemmin, U., Huwald, H., Selker, J. S., and Meneveau, C.: Subgrid-scale dynamics of water vapour, heat, and momentum over a lake, Boundary-Layer Meteorology, 128, 205–228, https://doi.org/10.1007/s10546-008-9287-9, publisher: Springer, 2008.

von Lindheim, J., Harikrishnan, A., Dörffel, T., Klein, R., Koltai, P., Mikula, N., Müller, A., Névir, P., Pacey, G., Polzin, R., and Vercauteren, N.: Definition, detection, and tracking of persistent structures in atmospheric flows, https://doi.org/10.48550/ARXIV.2111.13645, 2021.

Wadler, J. B., Zhang, J. A., Rogers, R. F., Jaimes, B., and Shay, L. K.: The Rapid Intensification of Hurricane Michael (2018): Storm Structure and the Relationship to Environmental and Air–Sea Interactions, Monthly Weather Review, 149, 245–267, https://doi.org/10.1175/MWR-D-20-0145.1, 2021.

Zhang, Y.-n., Wang, X.-y., Zhang, Y.-n., and Liu, C.: Comparisons and analyses of vortex identification between Omega method and Q criterion, Journal of Hydrodynamics, 31, 224–230, 2019.